Chapter 6
3D Test Cases

6.1 Introduction

This chapter details the results obtained with the new transition model for a variety of 3D aeronautical and turbomachinery flows. The 3D aeronautical test cases include the transonic DLR F-5 wing (shock induced laminar separation/turbulent reattachment, Sobieczky, 1994) and qualitative results for a full helicopter body (natural transition on the fuselage, bypass transition on the tail surfaces buffeted by the fuselage wake). The 3D turbomachinery test cases include an annular compressor cascade (RGW, Schulz and Gallus, 1988), a GE low-pressure turbine blade, an NREL wind turbine (Simms et al., 2001) and a generic transonic fan blade for a jet engine. All simulations have been computed with CFX-5.

The best practice grid guidelines for the transition model (see Appendix) were used to generate all of the grids. As a result, the grids in the computations had a maximum y^+ of approximately one, wall normal expansion ratios between 1.1 and 1.2 and at least 100 nodes were present in the streamwise direction in order to properly resolve the laminar, transitional and turbulent boundary layers. A summary of the inlet conditions for all the test cases described in this chapter is given in Table 6.1. Where possible, the inlet turbulence levels were specified in order to match the experimentally measured FSTI. If the freestream turbulence was not known in the experiment than an educated guess was made for the inlet values such that at the leading edge of the body the values were representative of a typical wind tunnel.

Case	$Re_x = \rho c U_o/\mu$ ($x10^6$)	Mach = U_o/a where speed of sound (a) = $(\gamma RT)^{0.5}$	Chord (m)	FSTI (%)	μ_t/μ
DLR F-5 Wing AoA = 2°	1.5	0.82	0.15	0.5	10
Eurocopter	30	0.12	11	0.05	1.0
RGW Annular Compressor	0.4	0.28	0.0626	1.25	2.0
GE Low-Pressure Turbine	0.1	0.6	-	5.0	31
NREL Wind Turbine	0.84 – 1.31	0.06 – 0.1	0.63	0.3	10
Transonic Fan	0.5, 1.0, 1.6	0.75	0.096	0.5	10

Table 6.1 Inlet conditions for the 3D test cases

6.2 Aeronautical Test Cases

6.2.1 DLR F-5 Transonic Wing

The DLR F-5 geometry is a 20° swept wing with a symmetrical airfoil section that is supercritical at a freestream Mach number of 0.82. The experiment was performed by Sobieczky (1994) and consists of a wing mounted to the tunnel sidewall (which is assumed to have transitioned far upstream of the wing). At the root the wing was designed to blend smoothly into the wall thus eliminating the horseshoe vortex that usually develops in the root area. The experimental measurements consist of wing mounted static taps at various spanwise locations and flow visualization of the surface shear using a sublimation technique. The grid used for the transitional computations consisted of 6 million nodes and is shown in Figure 6.1. Both the wing and the tunnel side wall had a viscous sublayer grid with a maximum y^+ of one.

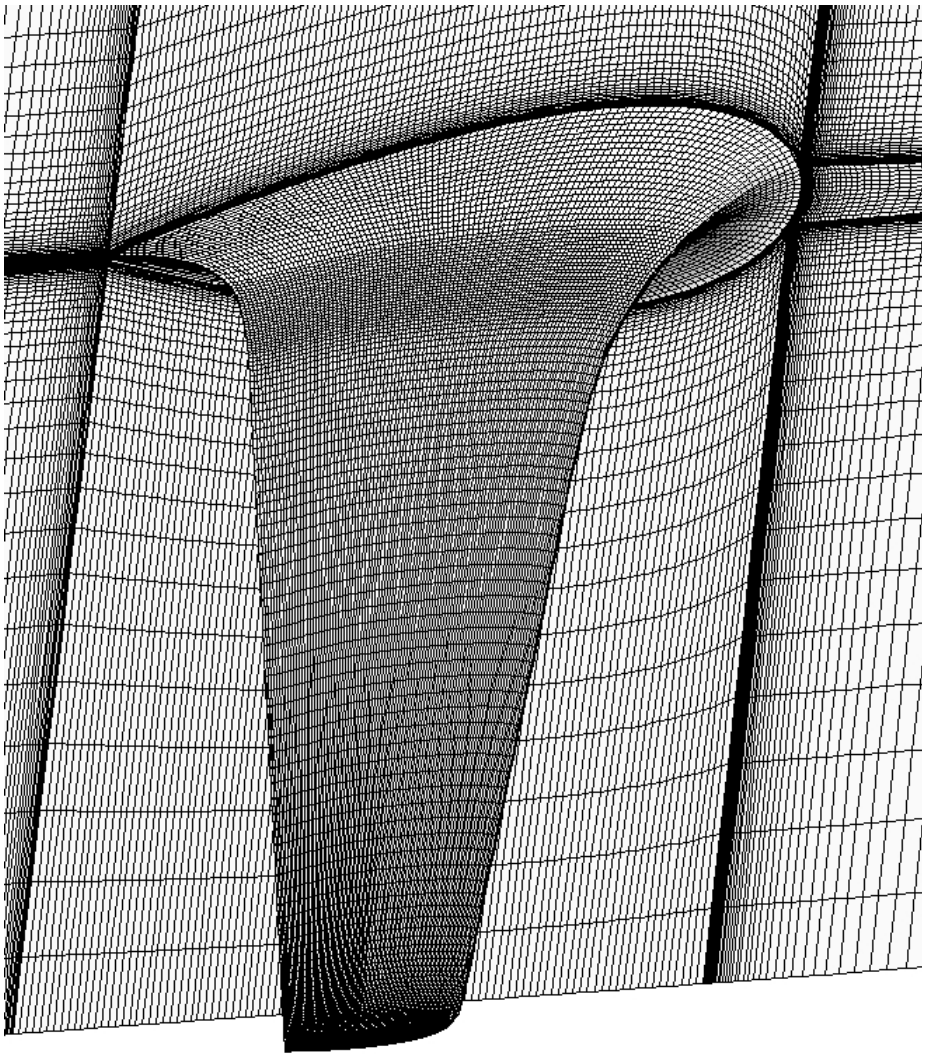

Figure 6.1 Close up of the grid used to compute the DLR F-5 wing.

The experimental flow visualization of the 2° angle of attack case is shown in Figure 6.2 (right). Based on the flow visualization and the pressure measurements a diagram of the flow field around the wing was constructed and can be seen in Figure 6.2 (middle). The measurements indicate that the boundary layer is laminar until about 60% chord where a shock causes the laminar boundary layer to separate and reattach as a turbulent boundary layer. The contours of skin friction and the surface streamlines predicted by the transition model are shown in Figure 6.2 (left). From the skin friction the laminar separation and turbulent reattachment positions can be clearly seen and both appear to be in very good agreement with the experimental diagram from about 20% span out to the wing tip. After the turbulent reattachment a strong increase in the pressure is observed, both in the experiment and in the CFD computation.

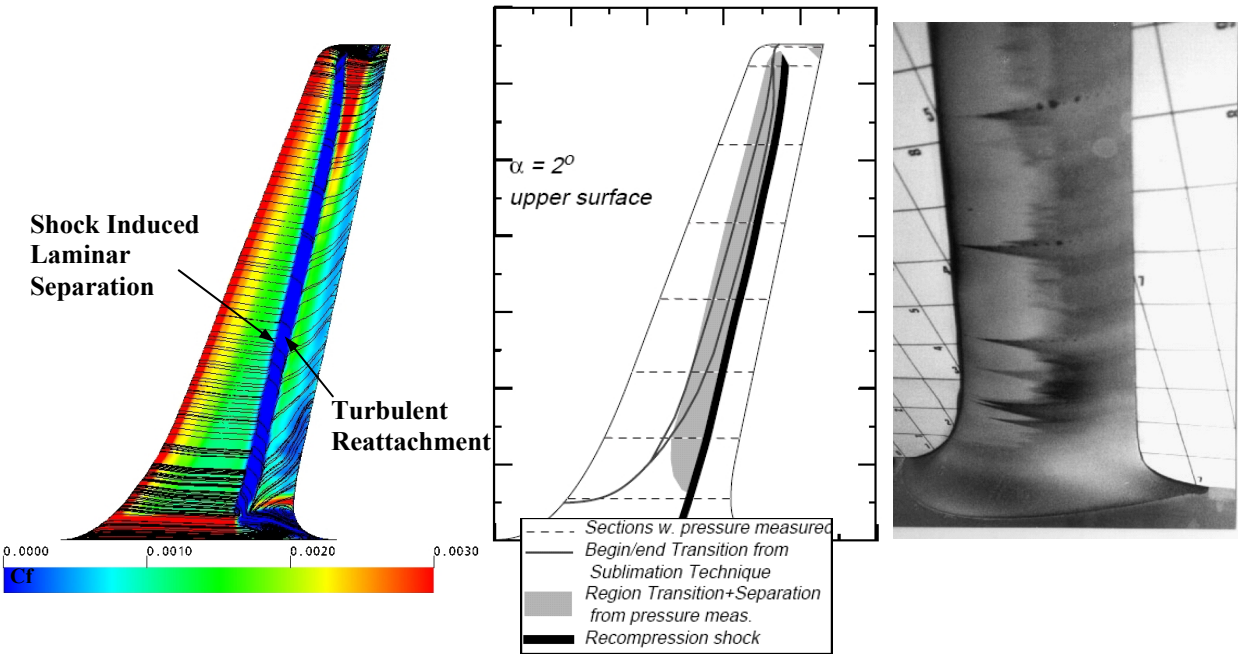

Figure 6.2 Contour plot of skin friction (Cf) and surface streamlines predicted by the transition model (left), experimental diagram of the flow field (middle) and experimental flow visualization of the surface shear on the DLR-F5 wing (right).
Experimental figures (middle, right) reproduced from Sobieczky (1994).

The predictions differ from the experiment at the wing root region as shown in Figure 6.3. In the CFD predictions there are two distinct transition regimes. The first regime is transition due to attachment line contamination where the turbulent boundary layer from the tunnel wall essentially convects along the leading edge of the wing and results in a fully turbulent boundary layer downstream of this stagnation region. This is in fact a very difficult phenomenon to predict with a transition model because it is essentially a convection dominated process. The transition model was able to predict this because it is based on locally formulated transport equations and local values for the transition

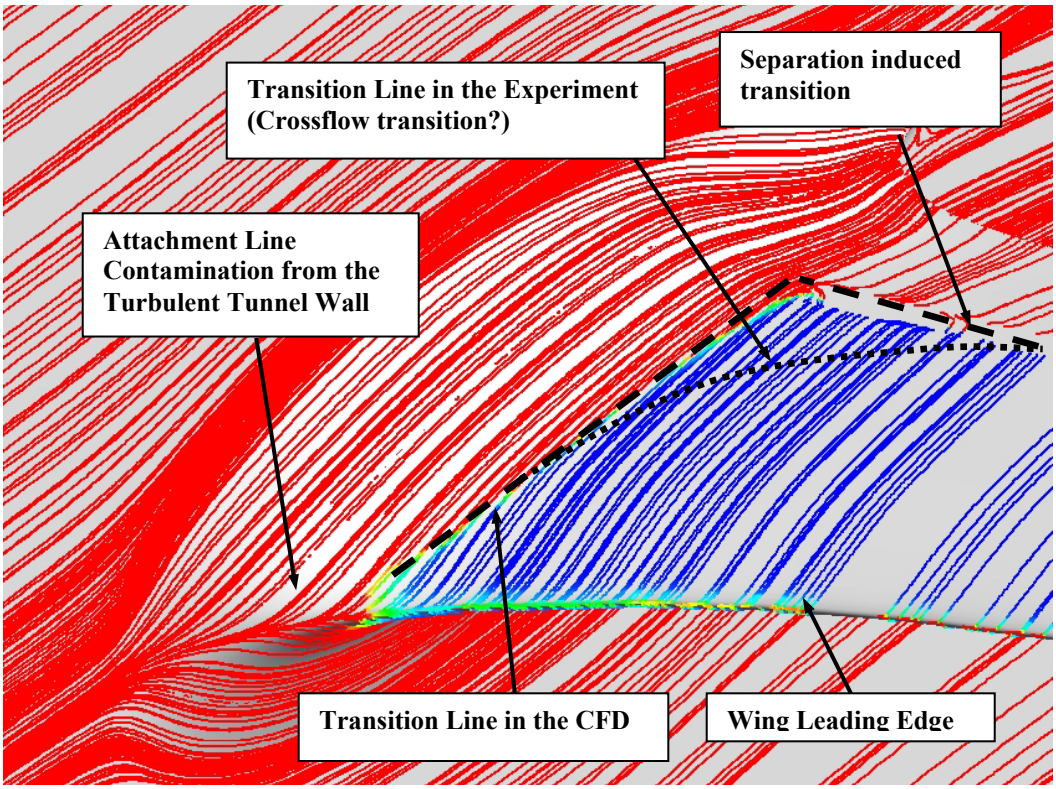

Figure 6.3 Surface streamlines at the DLR-F5 wing root colored by the local intermittency: blue = laminar, red = turbulent.

indicators. As a result it can naturally account for the convection of a turbulent boundary layer and its effect on transition.

The second transition regime is caused by a shock-induced laminar separation and there is an abrupt switch between the two modes in the CFD predictions. However, based on the experiment the transition line appears to smoothly switch from the separation induced mode to the attachment line contamination mode. It is possible that this smooth change is actually crossflow induced transition as the angle between the surface streamlines and the freestream velocity is significant in this region. The current empirical correlations do not account for crossflow effects and as a result, it is not surprising that differences occur in this region. It should be noted that this is not a conceptual weakness of the present approach because in principle the effect of crossflow instability could be included in the empirical correlations for transition onset.

6.2.2 Eurocopter Airframe

The Eurocopter airframe is a 3-dimensional helicopter configuration that would typically be used to investigate the drag coefficient of a proposed helicopter design (minus the influence of the rotor blades). At present, there is no experimental data available in the open literature on this geometry. Nevertheless, it is still an interesting test case for the

transition model because of it's complexity and because it represents an actual industrial geometry. The primary interest is in comparing the fully turbulent solution to the transitional solution and in demonstrating that the transition model does not adversely affect the convergence and robustness of the underlying flow solver. The grid for this case consisted of about 6 million nodes and the farfield was located ten helicopter lengths away. Each solution was run overnight in parallel on a 16 CPU Linux cluster. The predicted skin friction for a fully turbulent and transitional solution is shown in Figure 6.4. The main differences in the transitional solution are that the front part of the fuselage, the two outside vertical tail surfaces and the outer half of the horizontal tail surface are laminar.

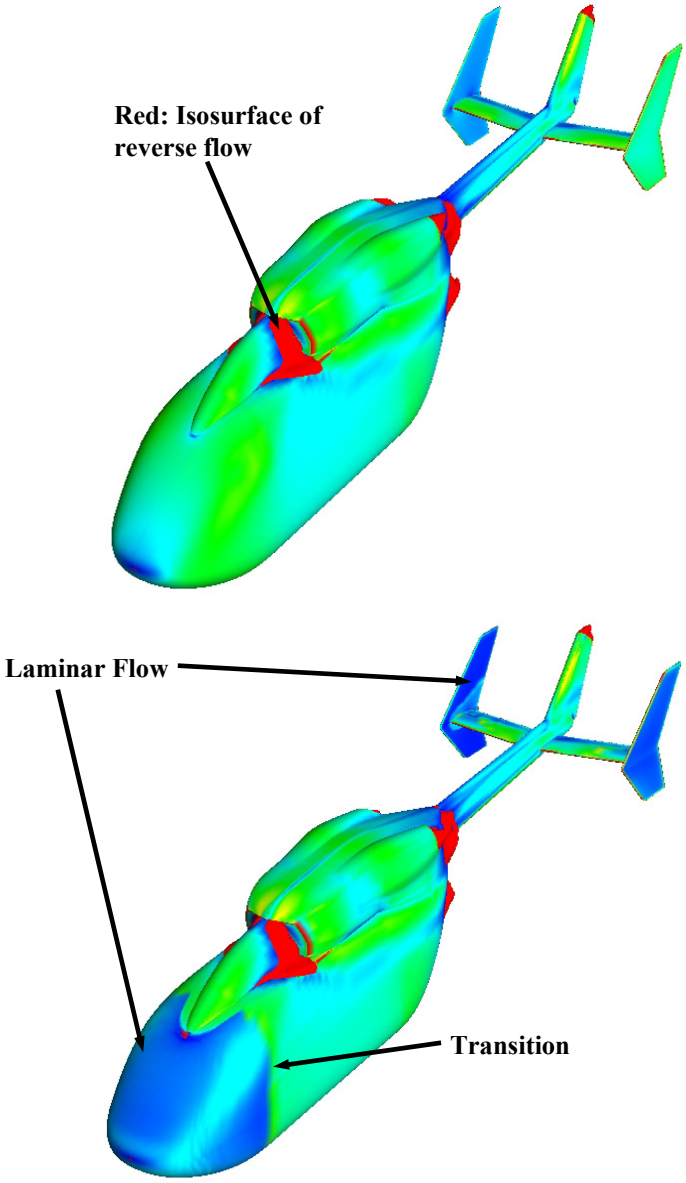

Figure 6.4 Contour plot of skin friction for a fully turbulent (top) and transitional (bottom) Eurocopter airframe.

The fact that the transition model predicted turbulent flow on the middle vertical stabilizer and the inner part of the horizontal stabilizer was unexpected. Further investigation revealed that this was caused by the turbulent wake that was shed from the fuselage upstream of the tail. This is best illustrated in Figure 6.5. The top picture shows an iso-surface of the turbulent flow. The turbulent wake is clearly visible and can be seen passing over the middle vertical stabilizer and the inner part of the horizontal stabilizer. Consequently, the transition model predicts bypass transition on these surfaces due to the high local freestream turbulence intensity from the wake. Outside the wake, the local freestream turbulence intensity is low and as a result the model predicts natural transition. This is a case where the local formulation of the transition model is a significant advantage because it allows the model to automatically account for large changes in the freestream conditions without requiring any outside input from the user.

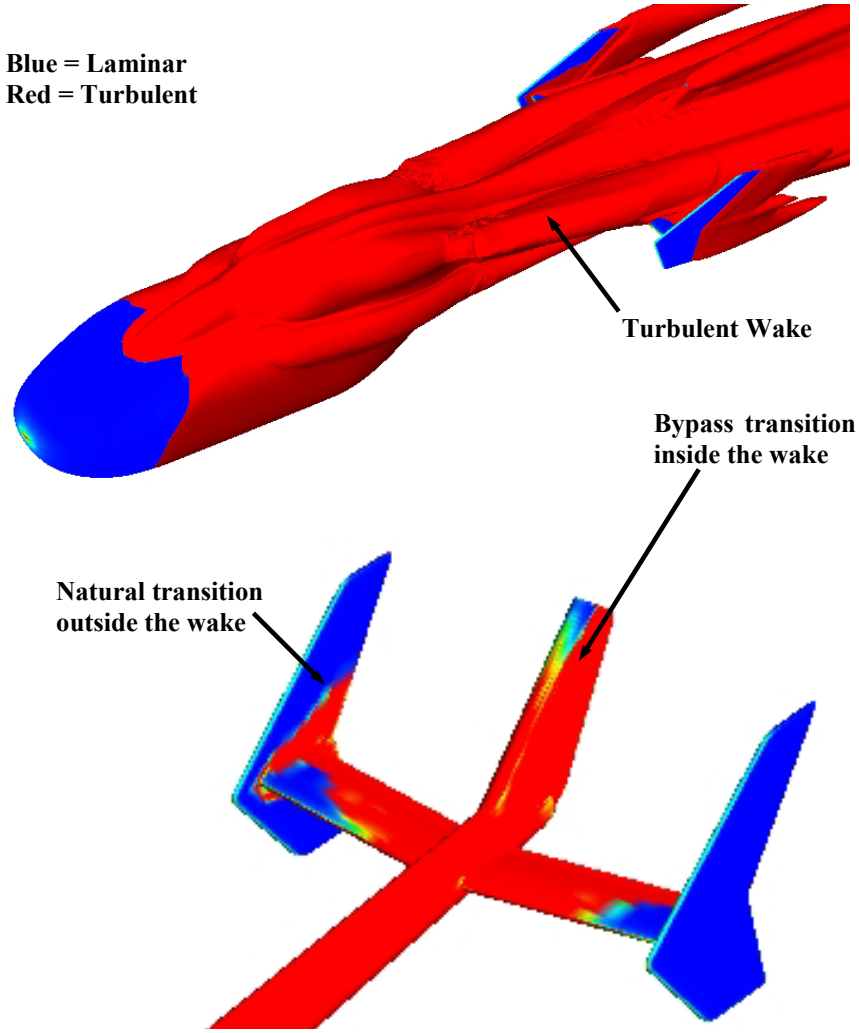

Figure 6.5 Iso-surface of turbulent flow (top) and surface value of intermittency (bottom) indicating the laminar (blue) and turbulent (red) regions on the Eurocopter airframe.

The convergence of lift and drag is shown in Figure 6.6 for the fully turbulent (top) and transitional (bottom) solutions. The transitional flow on the fuselage and tails resulted in a 5% drag reduction compared to the fully turbulent solution. A slight oscillation of the separation zones behind the engine compartment prevented a full residual convergence. However, the force convergence demonstrates that the transition model does not have any adverse effects on the robustness on the underlying CFD Code. Similar observations were made for the other testcases. The extra CPU cost of the transition model is around 17 percent compared to a fully turbulent solution on the same grid.

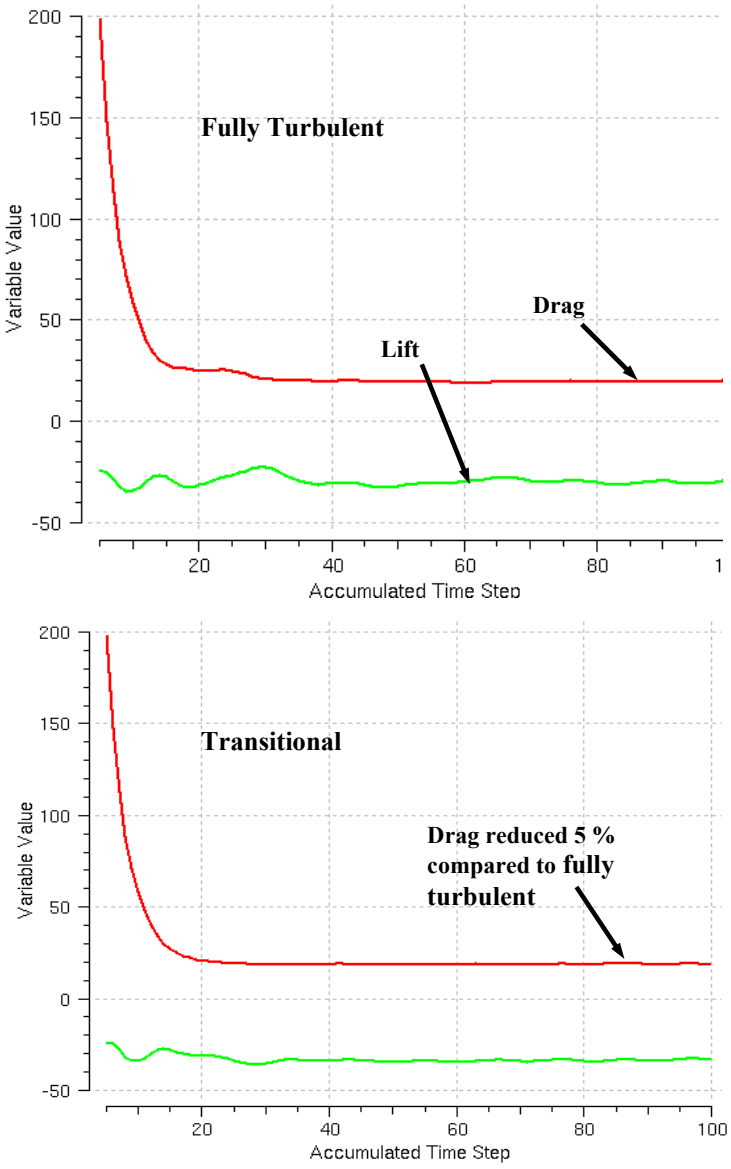

Figure 6.6 Convergence of lift and drag for the fully turbulent (top) and transitional (bottom) Eurocopter solutions.

6.3 Turbomachinery Test Cases

6.3.1 RGW Low-Aspect Ratio Annular Compressor Cascade

The first 3D turbomachinery test case is the RGW annular compressor cascade which was experimentally investigated by Schulz and Gallus (1988). It is a fully three-dimensional flow including sidewall boundary layers originating upstream of the blade. This flow topology poses a major challenge to standard correlation-based transition models, as complex logic would be required to distinguish between the different boundary layers (Thermann et al., 2001). The operating point was for a mean inlet flow angle of 44.2°. The geometry in the experiment is representative of a typical a compressor stator and consequently there are no gaps in between the tip and the casing. As well, the hub, blade and casing are stationary and thus system rotation does not need to be used. The grid used in the computation is shown in Figure 6.7 where the surface grid on the hub and blade are shown along with lines indicating the extent of the computational domain. There were 200 nodes around the blade, 60 normal to the blade surface and 60 in the span wise direction and the total grid size was about 900 000 nodes. The maximum RMS residual was 10^{-4} for the momentum equations. This is on the high side of what is generally considered acceptable and is probably due to the large regions of separated flow present on the suction side of the blade. The forces on the blade appeared to be steady and so the case was judged to be converged.

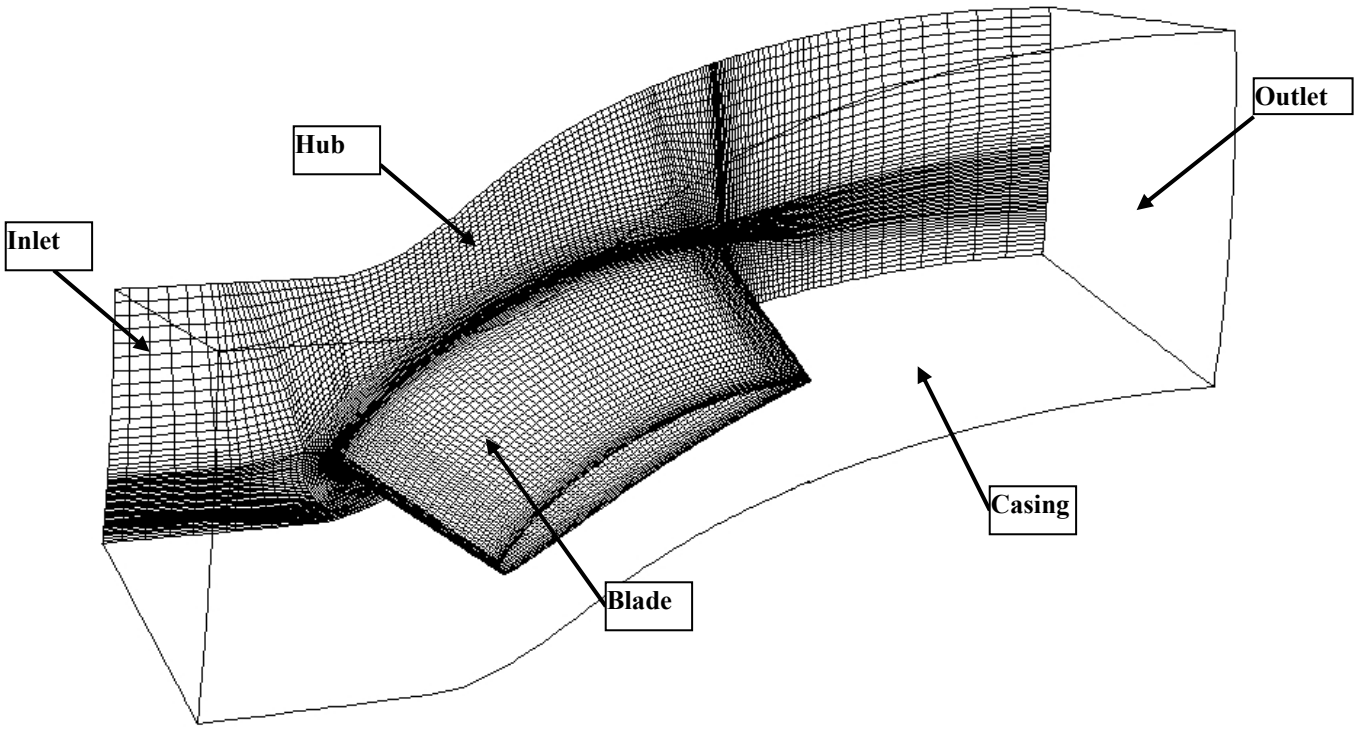

Figure 6.7 Grid for the RGW compressor cascade

Figure 6.8 shows a comparison of the simulations on the suction side of the blade with an experimental oil-flow picture. For comparison, a fully turbulent flow simulation is also included. The transition model captures the complex flow topology of the experiments in good qualitative agreement with the data. A comparison between the transition model and the fully turbulent simulation shows the strong influence of the laminar flow separation on the sidewall boundary layer separation. The flow separation on the shroud is significantly reduced by the displacement effect of the separation bubble in the transitional simulation. As a result, the loss coefficient (Yp) in the fully turbulent simulation of 0.19 is much higher than the experimental value of 0.097. The simulation with the transition model gives a value of 0.11 in much closer agreement with the experiment.

The main difference between the simulations using the transition model and the experimental oil-flow lies in the reduced laminar separation zone observed in the simulations. It results from a downstream shift of the laminar separation line. Similar discrepancies have been observed by Thermann et al. (2001) using an extended Mayle (1991) criterion for transition. The main reason for the delayed laminar separation does not necessarily come from the transition model, as it is not activated until after the separation occurs. The flow exhibits a complex interaction between the turbulent separation on the sidewalls and the location of the laminar separation line. It appears that the turbulent separation zones on the hub and especially on the shroud are overestimated in the simulation. This results in an acceleration of the core flow, which in turn could be the cause of the delay in the laminar separation, as it reduced the strength of the adverse pressure gradient at the center of the blade. However, from the pressure distribution (Figure 6.9) the suction side matches the experiment while there is clearly a difference between the experiment and the computation on the pressure side. As a result, there appear to be discrepancies either in the blade geometry or inlet flow conditions between the experiment and the computational setup and these discrepancies should be investigated further to determine their source.

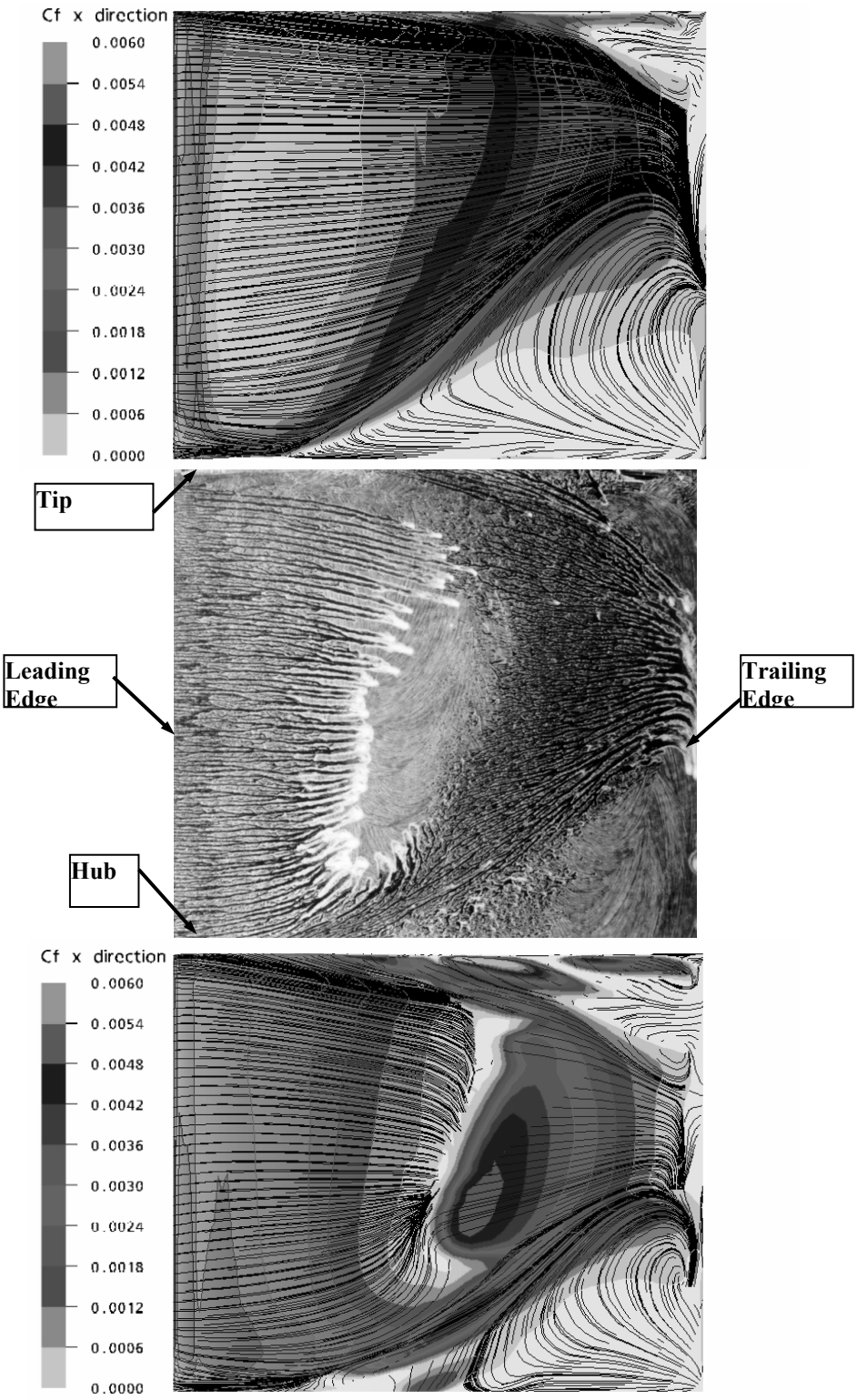

Figure 6.8 Fully turbulent (top) and transitional (bottom) skin friction on the suction side of the 3D RGW compressor cascade compared to experimental oil flow visualization (middle, from Schulz and Gallus (1988), Institute of Jet Propulsion and Turbomachinery, RWTH Aachen University).

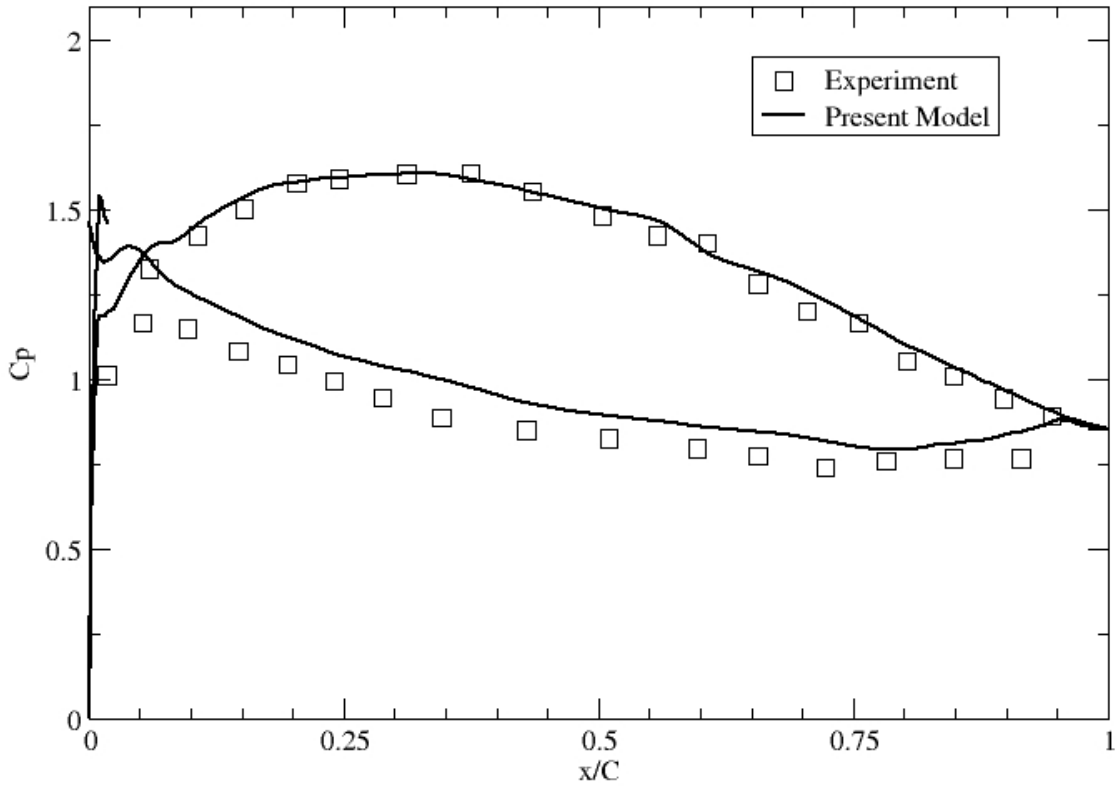

Figure 6.9 Cp distribution at mid-span for the 3D RGW compressor cascade.

6.3.2 NREL Phase VI Wind Turbine

The NREL Phase VI experiment consisted of a two-bladed twisted and tapered 10-meter diameter wind turbine that used the S809 airfoil section, which is shown in Figure 6.10. The NREL Phase VI wind turbine was tested in the NASA Ames Research Center 80-by-120 Foot Wind Tunnel and a large matrix of performance and load data was collected (Simms et al., 2001). In this study the main focus was only to compare the predicted torque output to the measured value and to investigate the differences between fully turbulent and transitional CFD solutions. The CFD grid for this case consisted of an O-type mesh of approximately 10 million nodes with a maximum y^+ of one. The grid used to compute the NREL wind turbine is illustrated in Figure 6.11. The second blade was modeled using a periodic boundary condition at the hub and farfield boundary conditions were located at approximately twice the rotor diameter. The inlet turbulence intensity specified for the CFD computations was 0.2%. Fully turbulent and transitional CFD runs were made for a wind speeds between 7 m/s and 25 m/s at a constant blade speed of 72 RPM (i.e. increasing angle of attack) and each run was computed overnight on a 16 CPU Linux cluster.

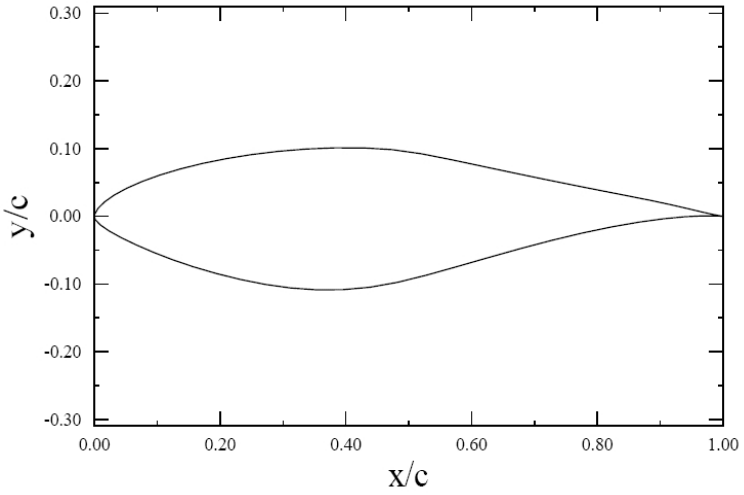

Figure 6.10 S809 Airfoil Profile

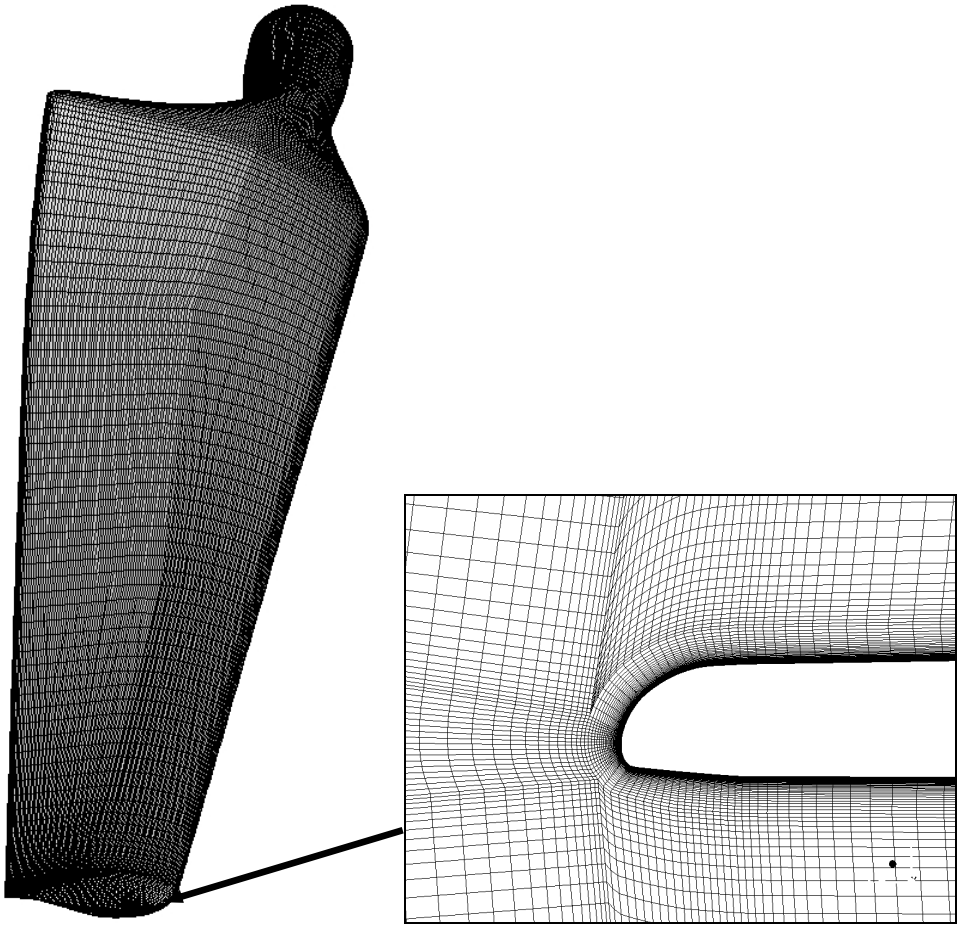

Figure 6.11 Grid used to compute the NREL Wind Turbine. Surface grid on the rotor (left) and close up of the volume grid near the tip (right).

The suction side streamlines and intermittency predicted by the transitional CFD computations for wind speeds of 7m/s, 10m/s and 20m/s are shown in Figures 6.12 and 6.13. As the wind speed is increased the effective angle of attack of the wind turbine increases because the blade rotation rate is held constant at 72 RPM. For the 7 m/s wind speed the flow is largely attached on the suction side. As well, a significant amount of laminar flow is predicted near the tip as well as in the hub region. In the tip region transition occurs at the 0.5 chord position whereas in the middle of the blade span transition occurs near the leading edge. This is most likely caused by the fact that the smaller radius results in an increased effective angle of attack. For the 10 m/s case the inner hub region stalls while the tip region remains attached up until the 0.5 chord position. As well, due to the increased angle of attack the transition location near the tip moves to the leading edge. Finally, at 20 m/s the suction side of the blade is completely separated and the intermittency contours indicate that the flow is almost completely turbulent.

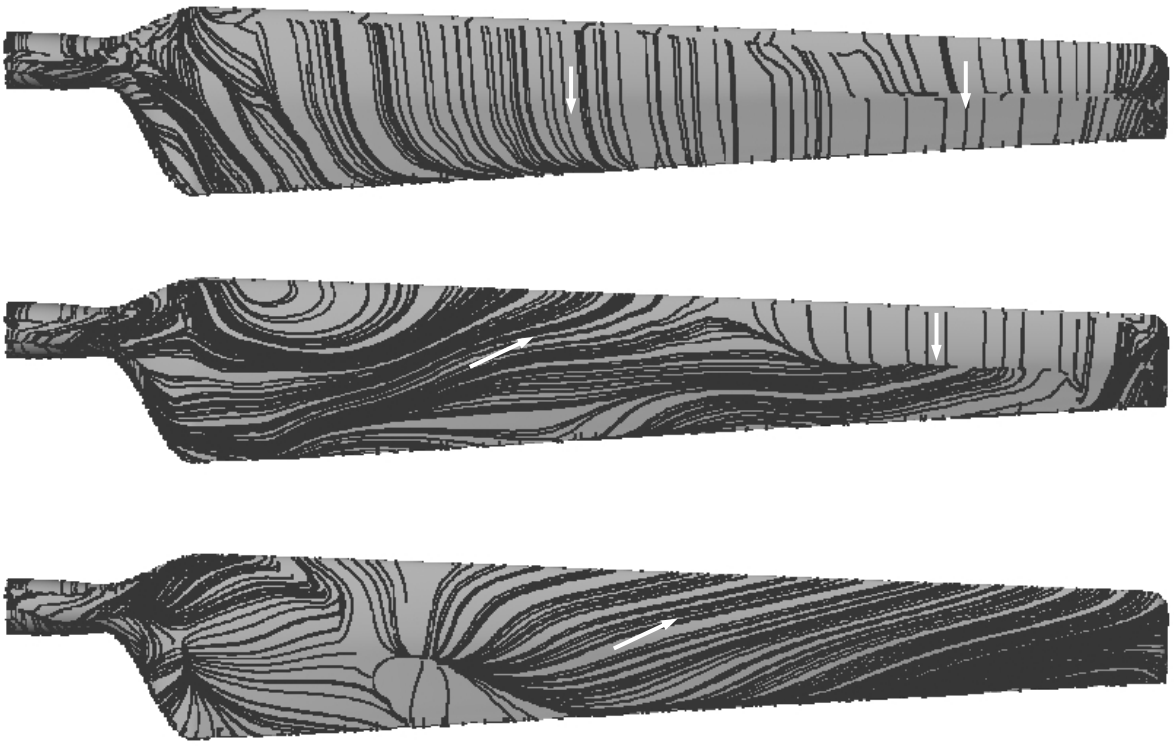

Figure 6.12 NREL wind turbine, suction surface streamlines computed with the transition model for wind speeds of 7m/s (top), 10m/s (middle) and 20 m/s (bottom). Arrows indicate flow direction.

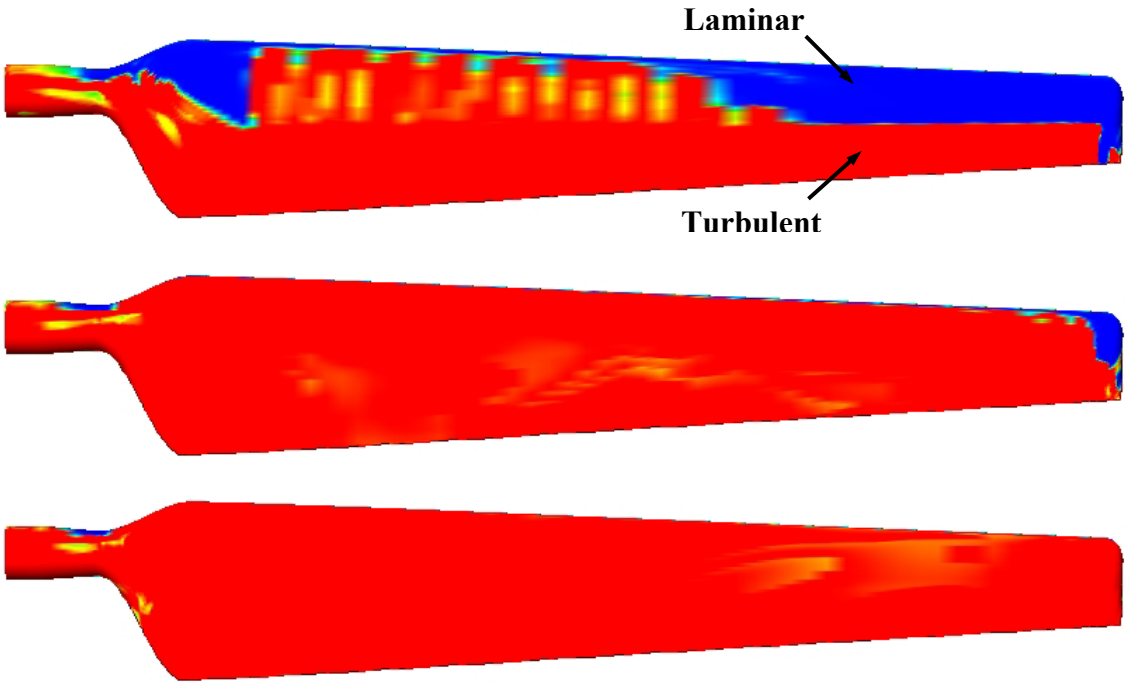

Figure 6.13 NREL wind turbine, suction surface intermittency computed by the transition model for wind speeds of 7m/s (top), 10m/s (middle) and 20 m/s (bottom). Note: blue indicates laminar flow and red indicates turbulent flow.

Figure 6.14 shows the predicted shaft torque in comparison with the experimental measurements. In general the agreement between the transitional CFD and experiment is quiet good considering how complex the flow field is on the suction side of the wind turbine. At a wind speed of 20 m/s there is a large difference between the transitional and fully turbulent shaft torque. Figure 6.15 is a contour plot of the local torque on the suction side computed for the fully turbulent and transitional solutions at this wind speed. The fully turbulent solution predicts much higher torque levels near the leading edge and also in the hub region.

The most likely explanation for this difference is the state of the boundary layer near the leading edge. At the 20 m/s wind speed the stagnation point is located on the pressure side and the suction side boundary layer must first travel up to and around the leading edge, at which point after the leading edge the boundary layer separates. For the transitional cases the boundary layer on the pressure side was laminar as it traveled from the stagnation point around the leading edge. It is well known that a laminar boundary layer will separate earlier than a turbulent boundary layer in a strong adverse pressure

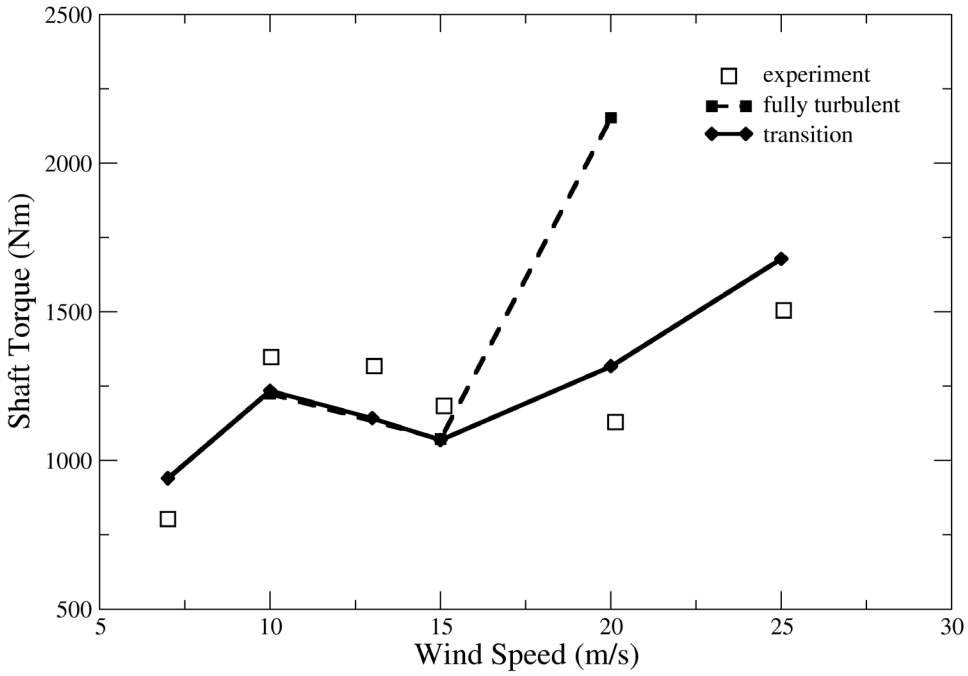

Figure 6.14 NREL wind turbine, predicted shaft torque at different wind speeds.

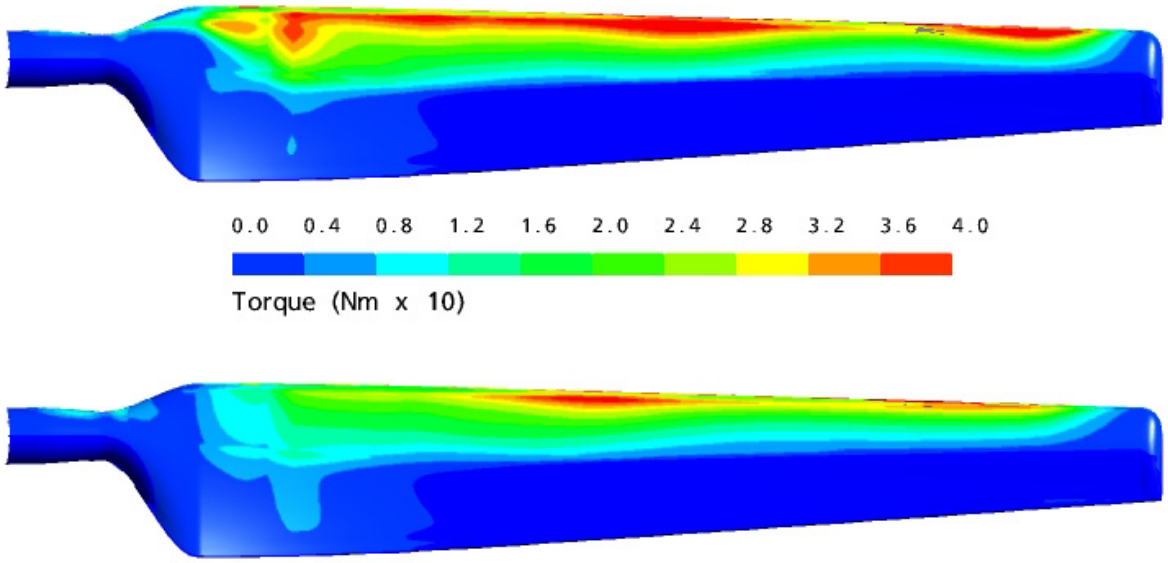

Figure 6.15 NREL wind turbine, local suction surface torque computed fully turbulent (top) and with the transition model (bottom) for a wind speed of 20 m/s.

gradient. Because of this, it would appear that as the boundary layer traveled from the stagnation point around the leading edge, the laminar boundary layer was not able to sustain as high a suction peak as the turbulent boundary layer. This would seem to be confirmed in Figure 6.16, which is a plot of the pressure distribution (Cp) at the 30 percent span location near the hub. The maximum suction peak Cp near the leading edge for the turbulent case was 9 while for the transitional case it was 5. After the suction peak the fully turbulent solution significantly over-predicts the Cp while the transitional solution is flat (indicating a strong separation after the leading edge) and is in relatively good agreement with the experimental measurements. It would appear that this could explain the 80% difference in output torque between the fully turbulent and transitional cases. It should be noted that other researchers have performed fully turbulent CFD computations of the NREL wind turbine and obtained relatively good results (e.g. Ref. 12). The separation near the leading edge is probably highly sensitive to the choice of turbulence model. The present fully turbulent results are thought to be accurate because they have been obtained with the well-known SST turbulence model, which is generally regarded as one of the best two-equation models available for predicting turbulent separation.

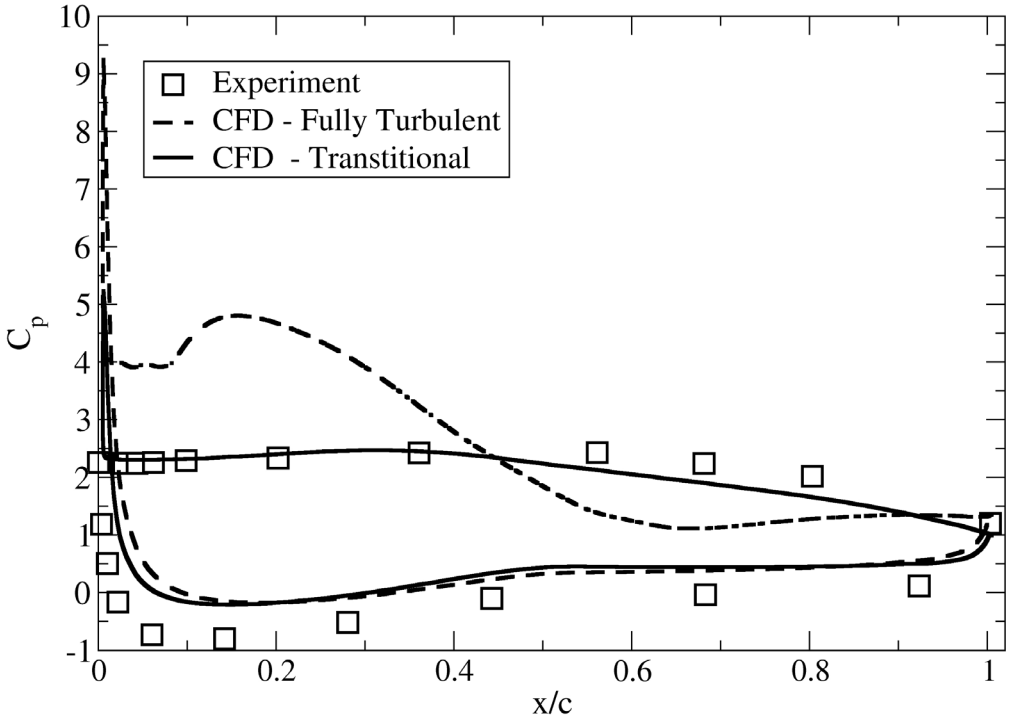

Figure 6.16 Pressure Distribution (Cp) for the NREL wind turbine at the 30 percent span location for a wind speed of 20 m/s.

6.3.3 GE Low-Pressure Turbine Vane

The next two test cases qualitatively investigates the behavior of the transition model for some actual industrial turbomachinery flows namely a GE Low Pressure Turbine Vane and a generic transonic fan blade. Because these are industrial geometries there is no experimental data available for either case in the public domain. The main purpose of these two studies is to show that the transition model functions correctly in a real industrial case and at the very least gives qualitatively reasonable results. The first test case is a GE Low Pressure Turbine Vane. In particular, the interaction of end-wall and vane boundary layers and the impact on the predicted transition location were of interest.

The convergence history for the fully turbulent and transitional computations is shown in Figure 6.17. There is some additional effort required for the transitional computation because the laminar boundary layers must first be resolved before the turbulent boundary layer starts to develop downstream of transition. However, overall the convergence with the transition model is very good.

Figure 6.18 shows wall-shear stress contours on the suction side of the vane and skin friction coefficients at various radial locations. It should be noted that the scales for the wall-shear stress contour plot and skin friction have been removed due to the sensitive nature of this geometry. The wall-shear contour plot (Figure 6.18b) indicates that away from the end-walls the suction side flow is laminar up to about 70% chord, where it transitions right before the laminar separation point. On the pressure side the flow was completely laminar. Figure 6.18c shows the friction coefficient at 50% span. For comparison, the friction coefficient from a fully turbulent computation is plotted as well.

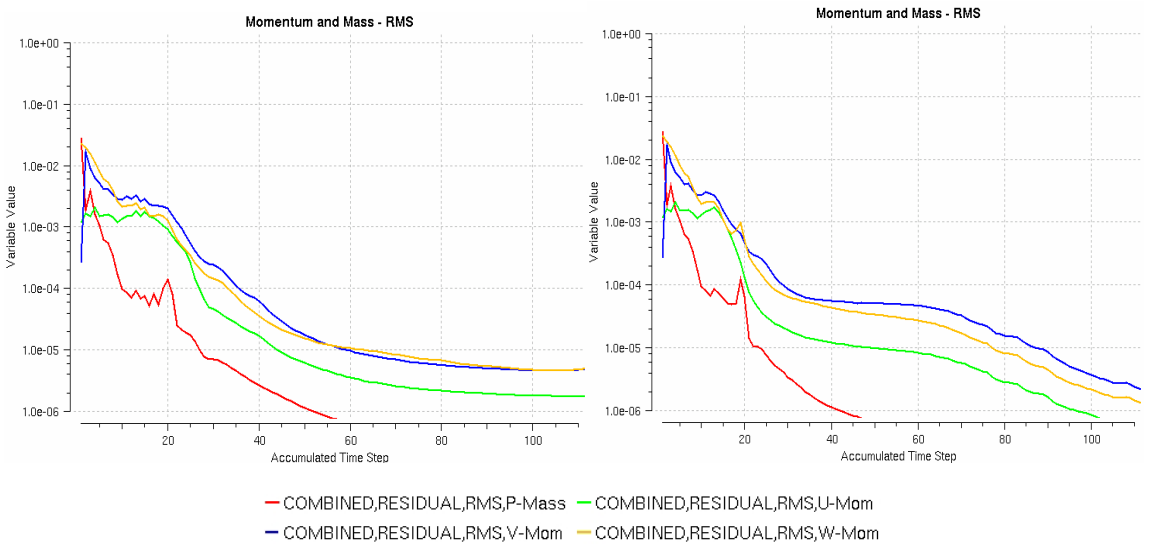

Figure 6.17 Convergence history for a low-pressure stator vane for a fully turbulent (top) and transitional (bottom) computation.

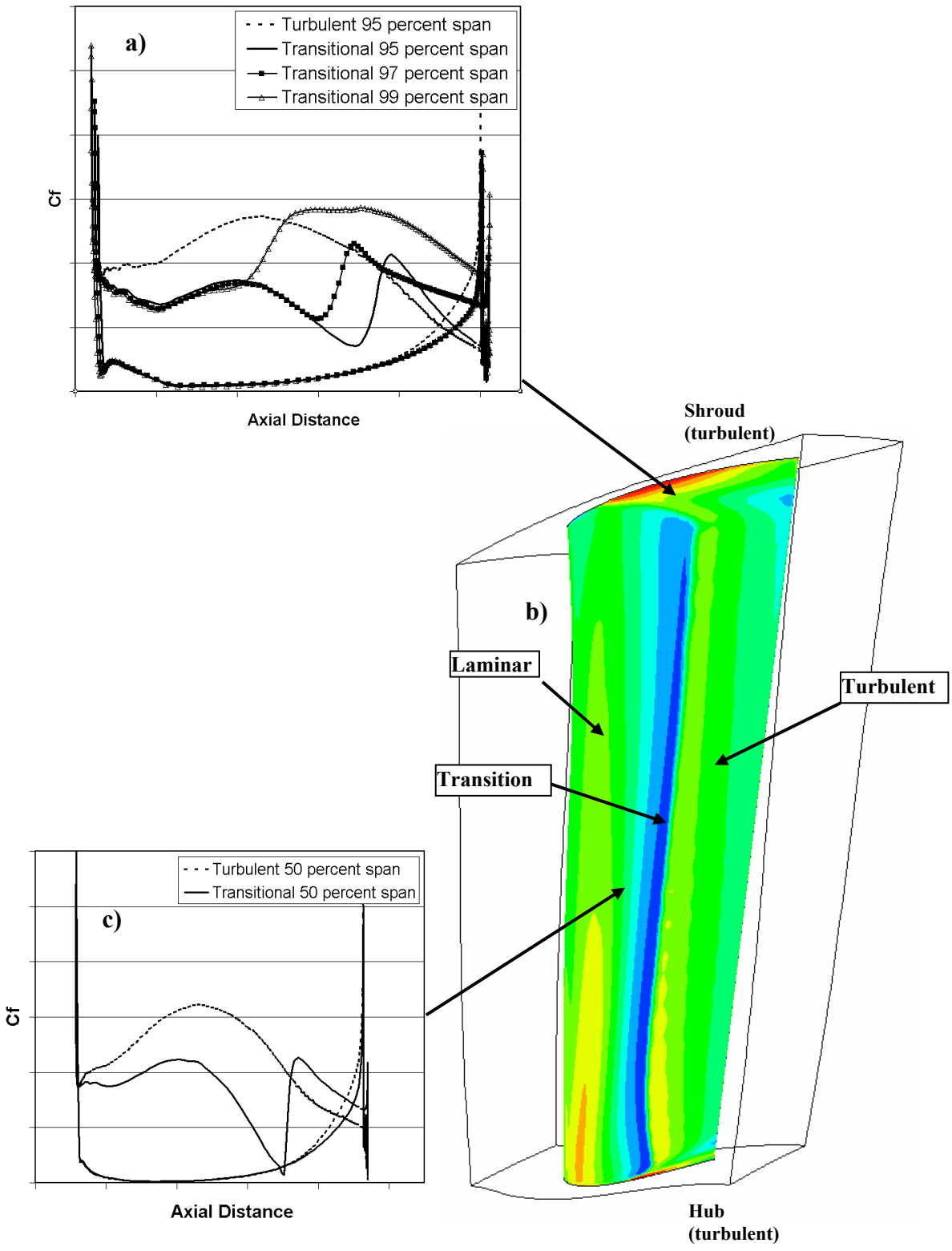

Figure 6.18 Predicted wall-shear contours and skin friction (Cf) for the GE Low-Pressure stator guide vane.

Figure 6.18a shows the effect of the end-wall boundary layer on the predicted transition location. Skin friction coefficients are plotted for 95%, 97% and 99% span. With increasing span, the vane boundary layer interacts more strongly with the fully turbulent end-wall boundary layer. As a result, the transition model sees higher levels of local turbulence intensity outside the vane boundary layer and transition is triggered further upstream.

6.3.4 Transonic Fan

The last test case in this chapter is a transonic fan for a gas turbine jet engine. The grid consisted of 6 million nodes and the geometry along with the surface grid on the fan blade is shown in Figure 6.19. For most typical engines at flight Reynolds numbers transition on the fan is usually not considered to be a significant issue. However, for small engines at high altitudes or wind tunnel tests at lower than flight Reynolds numbers transitional effects can become significant. If the Reynolds numbers are low enough a significant amount of laminar separation can occur resulting in blade flutter or even stall/surge. As well, a unique issue for the fan blades in an engine is that there are no upstream blade rows to generate freestream turbulence intensities at bypass transition levels. As a result, it is not unreasonable to expect a certain amount of natural transition and hence a significant amount of laminar flow on the blade surface. This case is an

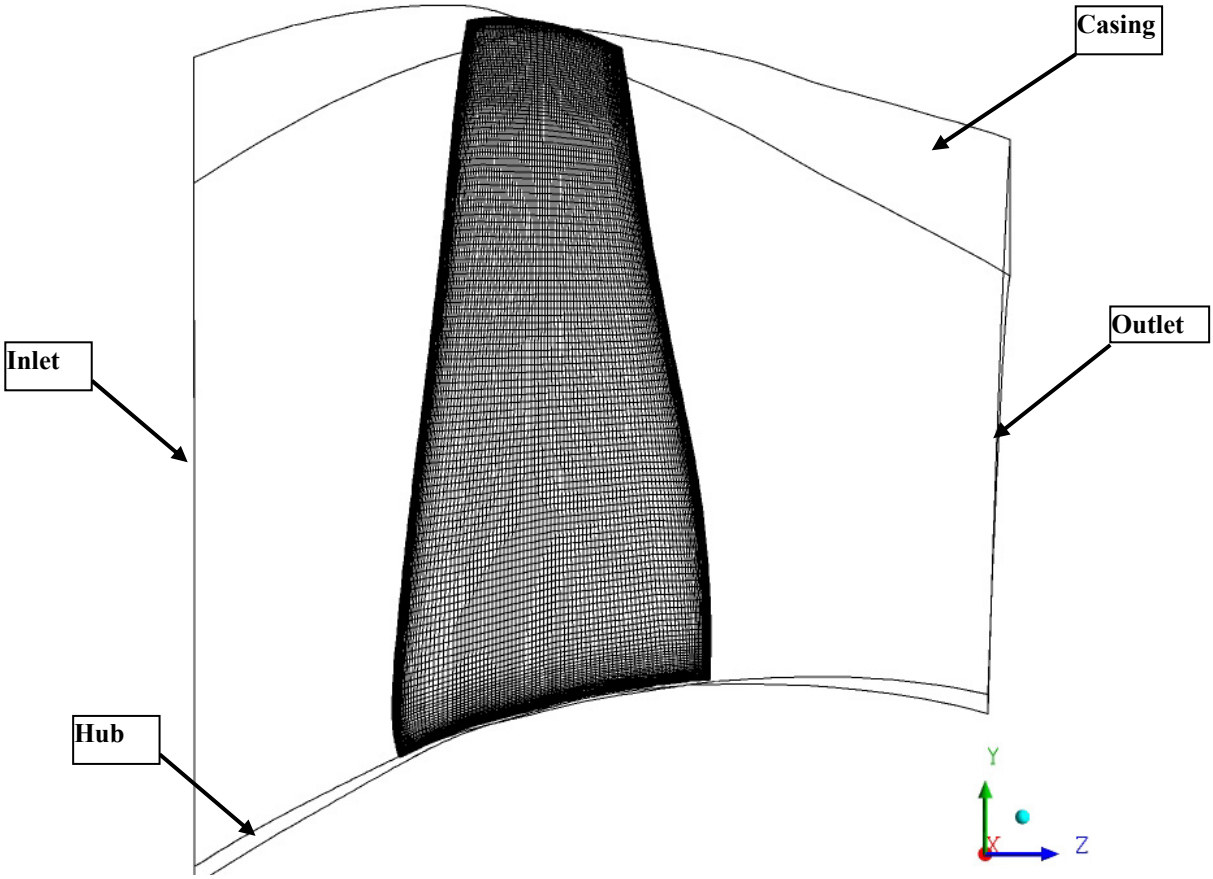

Figure 6.19 Pressure side view of the grid used to compute the Transonic Fan case.

industrial geometry and as a result there is no experimental data available for comparison in the public domain. The goal of the present test case is to investigate the effect of Reynolds number on the fan aerodynamics and to compare the results obtained for fully turbulent and transitional solutions.

In the present case the fan blade was run at Reynolds numbers of 1.6, 1.0 and 0.5 million which roughly corresponds to engine flight Reynolds numbers at altitudes of 0, 20 000 and 40 000 ft respectively. The wall shear and predicted surface streamlines on the pressure side for both fully turbulent and transitional computations are shown in Figure 6.20. For the fully turbulent cases there is no significant difference in the solutions as the Reynolds number is reduced. For the transitional case at a Reynolds number of 1.6 million transition occurs at about 60% chord. As the Reynolds number is reduced the transition location moves downstream until at a Reynolds number of 0.5 million the pressure side is completely laminar.

The wall shear and predicted surface streamlines on the suction side of both the fully turbulent and transitional computations are shown in Figure 6.21. At the lower 50% span near the hub there is a leading edge separation in all cases. Consequently, for the transitional cases the flow is tripped near the leading edge and thus the turbulent and transitional solutions are virtually identical in the lower 50 percent span of the blade. At the outer 50 percent span near the casing there is a strong shock that forces the boundary layer to separate in both the turbulent and transitional cases. In the transitional cases the shock induced separation also acts like a trip and thus the flow is laminar upstream of the shock and turbulent downstream of the shock. This can be seen in the surface values of intermittency shown in Figure 6.22. What is unique for this case is that the leading edge and shock induced separations are essentially fixed in location due to the geometry and are relatively insensitive to the change in Reynolds number. As a result, the suction side transition locations are very similar at the different Reynolds numbers. The increased amount of separation at the lower Reynolds numbers is mainly due to Reynolds number effects on the turbulent boundary layers rather than due to transitional effects.

The predicted loss coefficients as a function of Reynolds number for the turbulent and transitional solutions are shown in Figure 6.23. As expected, the loss coefficients are larger at the lower Reynolds numbers due to the increased viscous losses. What was surprising was that at the lower Reynolds numbers the transitional loss coefficient was smaller than the fully turbulent one. One potential explanation could be that the laminar boundary layer on the pressure side of the transitional solution reduced the viscous losses compared to the fully turbulent solution. Since the turbulent and transitional cases had similar separation points on the suction side, the reduced pressure side losses could explain the differences in loss coefficients at the lower Reynolds numbers.

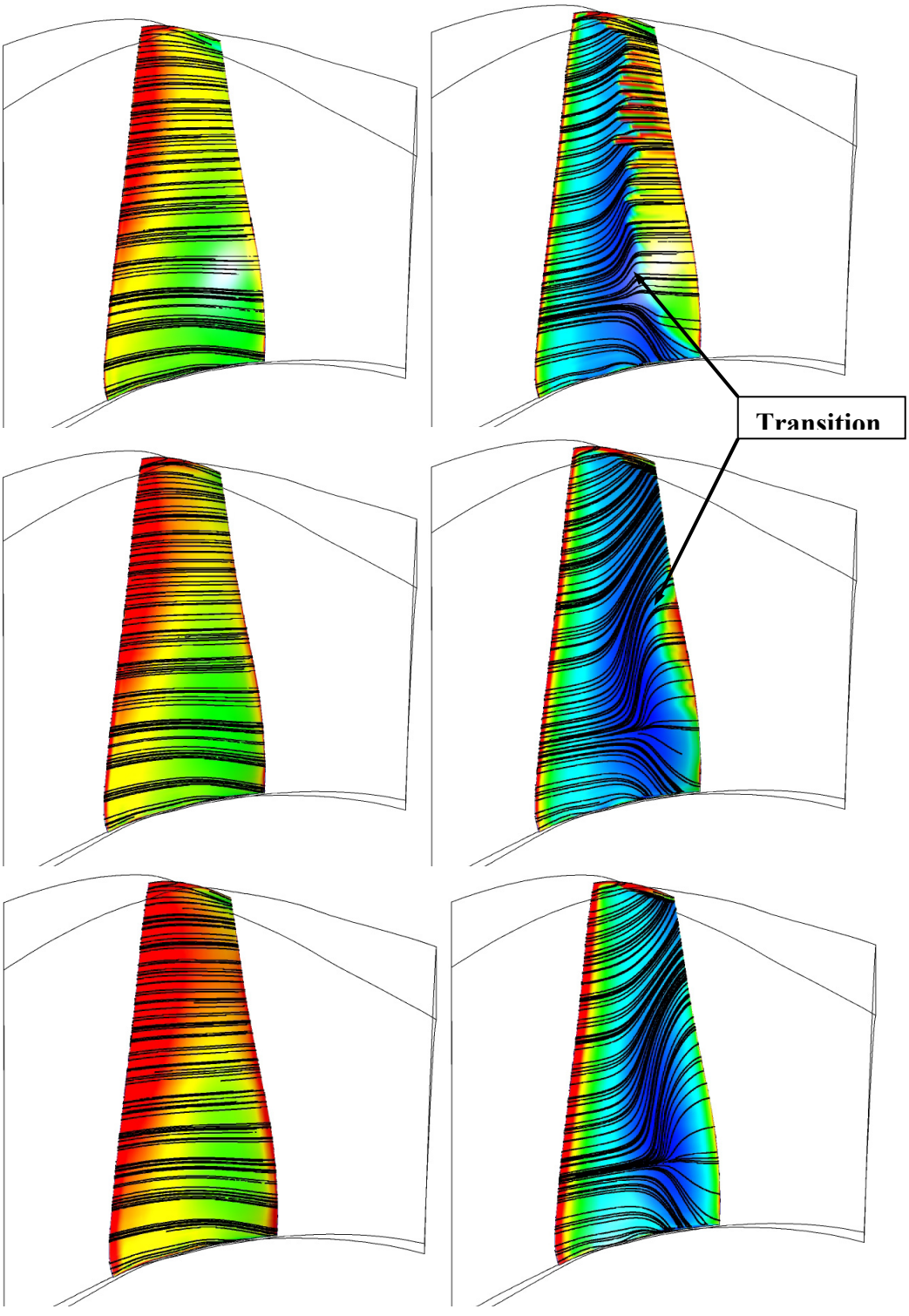

Figure 6.20 Comparison of full turbulent (left) and transitional (right) wall shear and surface streamlines on the pressure side of the Fan blade for Reynolds number of 1.6 (top), 1.0 (middle) and 0.5 (bottom) million.

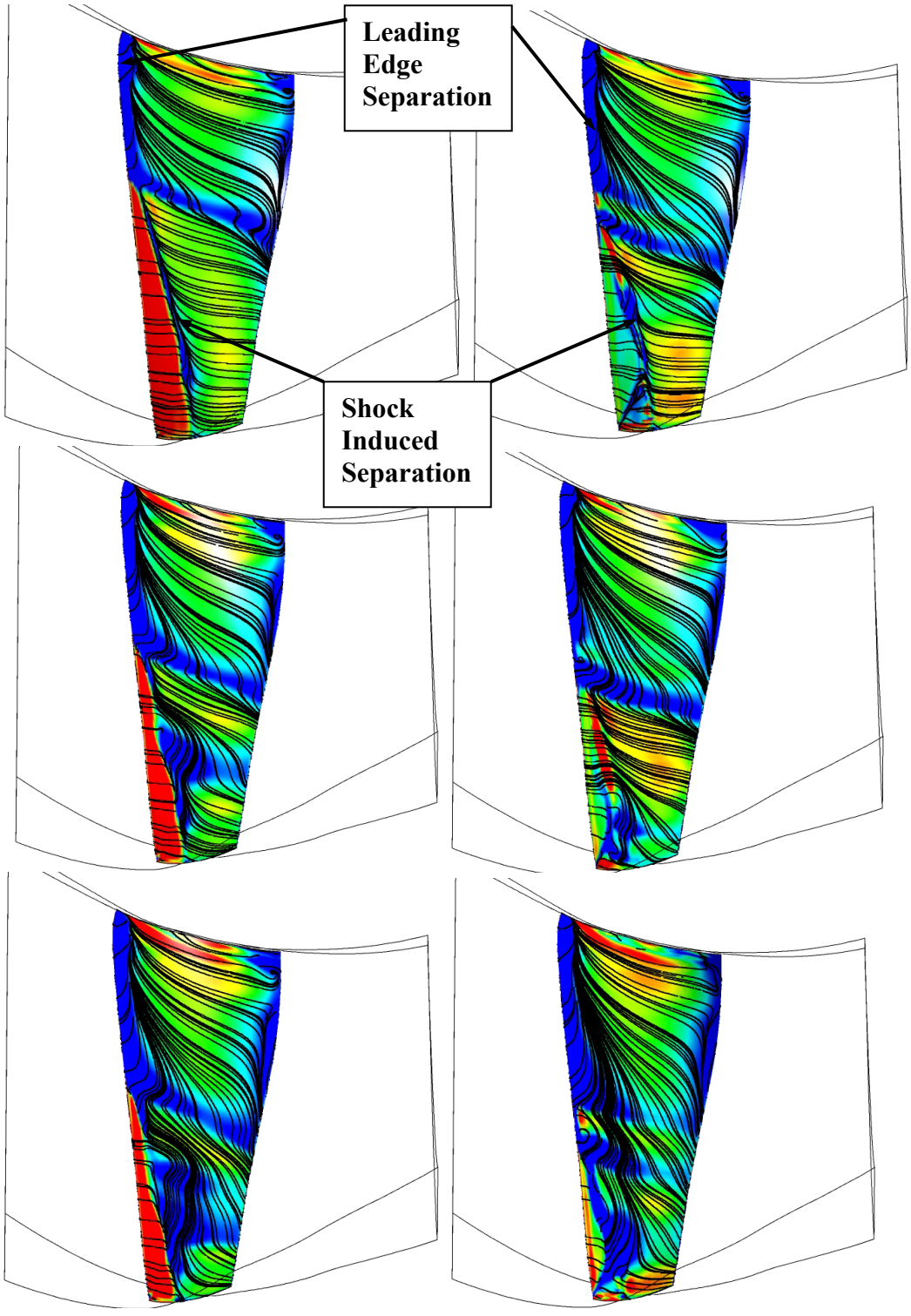

Figure 6.21 Comparison of full turbulent (left) and transitional (right) wall shear and surface streamlines on the suction side of the Fan blade for Reynolds number of 1.6 (top), 1.0 (middle) and 0.5 (bottom) million.

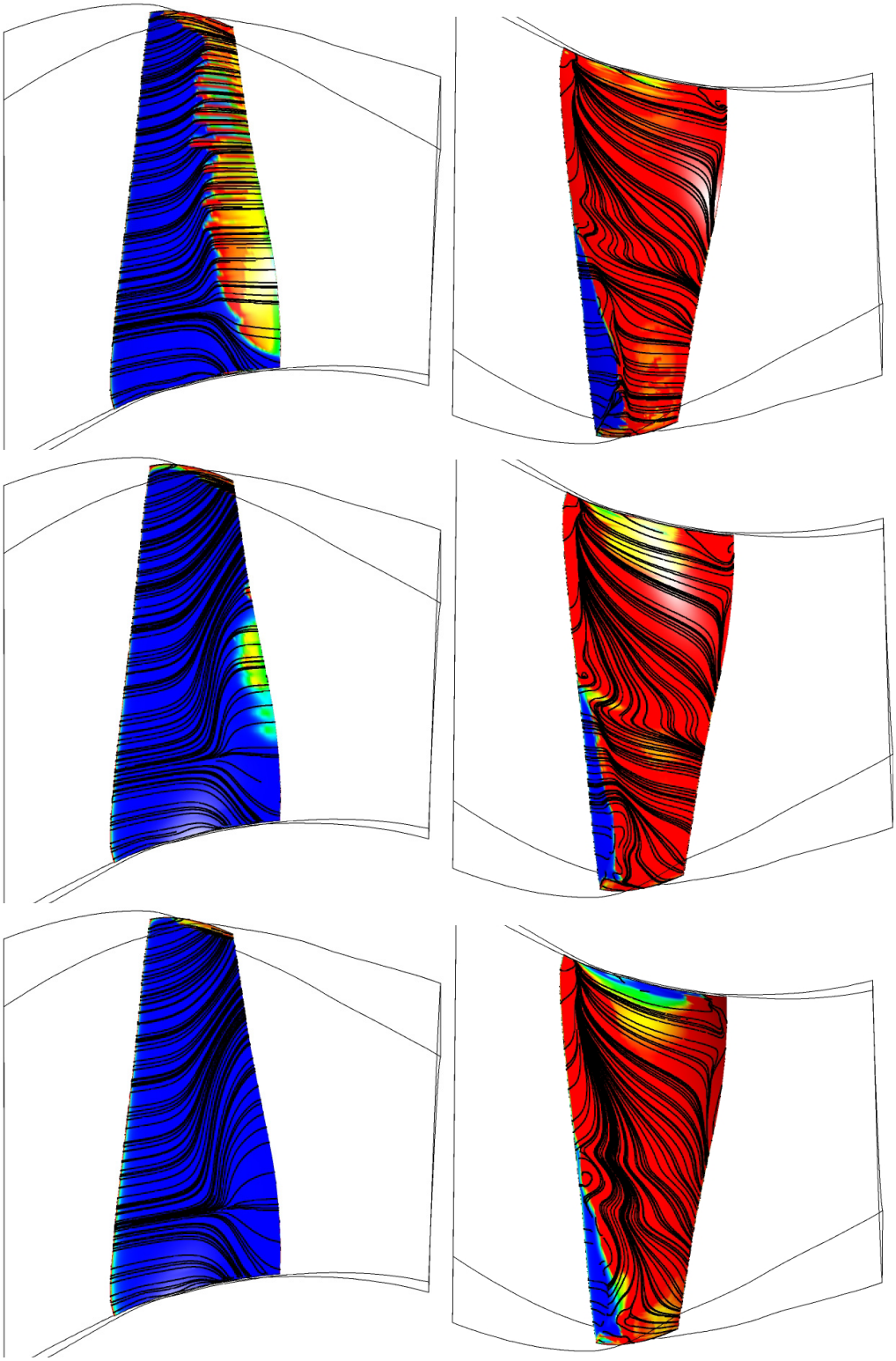

Figure 6.22 Comparison of pressure side (left) and suction side (right) surface intermittency and surface streamlines for the Fan blade at Reynolds numbers of 1.6 (top), 1.0 (middle) and 0.5 (bottom) million.

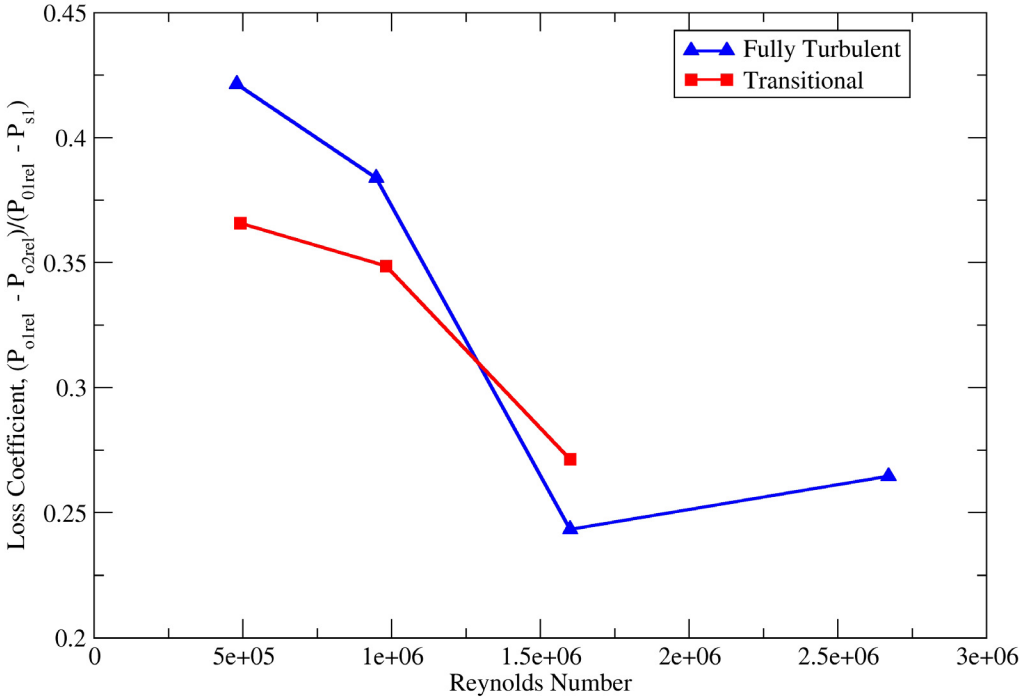

Figure 6.23 Loss Coefficient as a function of Reynolds number for the fully turbulent and transitional fan blade solutions.

This concludes the chapter on the 3-D test cases for the transition model. Unfortunately there is not nearly as much experimental data available that can be used to validate the model for the 3-D test cases as was available for the 2-D cases. There is clearly a need for more experimental data on 3-D transition that is openly accessible. The flow visualization for the DLR-F5 and RGW cases was obviously very useful in this regard. With respect to these two cases, very good agreement with the available experimental data was obtained. As well, the NREL wind turbine transitional results were also in relatively good agreement with the experimental measurements. Transitional effects on the wind turbine appear to explain why the torque output was over predicted by the fully turbulent simulations. Finally, experimental data for the Eurocopter airframe, GE low-pressure turbine vane and the transonic fan blade was not available. Consequently, it was not possible to perform a detailed validation with experimental measurements. Nevertheless, the transition model predictions for all three cases appeared to be reasonable.

Chapter 7
Conclusions and Recommendations

In this thesis a new correlation based laminar-turbulent transition model has been developed, which is built strictly on local variables. As a result, the transition model is compatible with modern CFD techniques such as unstructured grids and massive parallel execution. The model is based on two transport equations, one for intermittency (i.e. the fraction of time the flow is turbulent) and one for a transition onset criterion in terms of momentum thickness Reynolds number. The proposed transport equations do not attempt to model the physics of the transition process (unlike e.g. turbulence models), but form a framework for the implementation of transition correlations into general-purpose CFD codes.

The major new idea behind the transition model was to use van Driest and Blumer's (1963) concept of the vorticity Reynolds number to control the source terms in an intermittency equation. Since the vorticity Reynolds number is a local parameter it avoids the need to integrate boundary layer quantities such as momentum thickness Reynolds number in order to determine the onset location of transition and hence where the intermittency production terms should be active. In addition, a new transport equation for the transition momentum thickness Reynolds number ($\overline{\mathrm{Re}_{\theta t}}$) has been developed. This transport equation eliminates the need for a search algorithm in order to find the local freestream conditions for the empirical correlation. The $\overline{\mathrm{Re}_{\theta t}}$ transport equation therefore allows for completely automatic predictions of transition while still using a correlation based approach. All that is required of the user is the correct inlet values for turbulence intensity and viscosity ratio. These two new ideas have eliminated the non-local operations required to apply empirical correlations for transition onset. Consequently, empirical correlations can now be used to predict transition on unstructured and parallelized Navier-Stokes codes. At present, the transition model has been developed for predicting transition under the influence of freestream turbulence intensity, pressure gradients and flow separation. The model has been calibrated empirically for use with the Menter (1994) SST model, which is a popular and robust two-equation turbulence model.

The transition model has been validated against a large number of diverse and challenging test cases. An incremental approach was used to validate the model, first on flat plates, then 2D airfoils/turbine blades and finally on to progressively more complicated test cases such as a 3D transonic wing, a low-aspect ratio compressor and a full wind turbine. In general good agreement with the available experimental data was observed. For the 2D airfoils the accuracy of the present model appears to be comparable

with the well-known e^N method (at least as it has been implemented in the X-foil panel method code of Drela, 1995). This in itself is a significant achievement because it should now be possible to predict, with relatively good accuracy, the 2D lift/drag coefficients of an airfoil at moderate Reynolds numbers using a Navier-Stokes code without any manual specification of the transition locations. As well, the transition model is not limited to 2D flows and as a result can easily be used to predict transition in 3D flows (as was demonstrated for the DLR-F5 wing and the NREL wind turbine). Another significant advantage of the present model is that it has been shown consistently to be very good at predicting separation induced transition. This is particularly important for predicting transition in turbomachinery flows where the Reynolds numbers tend to be lower (and hence laminar separation more likely) than for the aeronautical cases. In fact, for a significant number of the turbomachinery test cases examined in this thesis, separation induced transition was the dominant transition mechanism. For the turbomachinery cases where bypass transition was present, the model was usually able to predict the transition location within about 5 percent chord of the experimental measurements.

One significant drawback of the new transition model is that it is not Galilean invariant. This is because the empirical correlations require the velocity in order to determine the turbulence intensity. For stationary or rotating reference frames this is not a problem as long as the relative velocity is used to compute the freestream turbulence intensity. However, when moving walls (i.e. sliding walls, deforming walls or walls rotating at a different speed compared to the rotating reference frame, e.g. the casing compared to a blade tip) are present then the freestream velocity relative to the wall will be in error. Galilean invariance is an important criteria for general turbulence models and any future work should therefore focus on improving this aspect of the model.

Another important area of transition that has not been addressed in great detail in this thesis is relaminarization. This phenomena is generally believed to occur when the acceleration parameter (K) exceeds 3×10^{-6} (Mayle, 1991). Such accelerations are common on the pressure side of most high-pressure turbines. Due to time constraints only a limited attempt has been made to test the transition model for relaminarization. Future attempts to validate the new transition model should therefore include an investigation into how accurately the model predicts this phenomenon. At present, this is not thought to be a major limitation in the present model, as the initial results were encouraging and many different low-Reynolds number turbulence models have been shown to be quite capable of predicting relaminarization without any additional modification.

A very interesting area for future development would be to extend the present model for predicting transition due to crossflow and roughness effects. On swept wings the dominant transition mechanism is actually crossflow induced transition, not natural transition. There exists a large body of work on crossflow transition and in principle, it should not be too difficult to extend the present empirical correlations for transition onset in order to account for the crossflow instability mechanism. As well, in-service gas turbine engines often have a significant amount of roughness, which increases with the service life. Roughness effects are thought to be quite significant in the high-pressure

turbine due to the impingement of the combustion products from the upstream combustion chamber. In principle, it should be relatively easy to include the effect of roughness into the empirical correlations for transition onset.

Finally, there is always a need to continue to validate the present transition model on additional test cases. The main limitation of the transition model right now is thought to be the accuracy of the empirical correlations. As more and more experimental data becomes available which can be used to calibrate the empirical correlations, the model accuracy should improve further. This is one of the main strengths of the present approach. With this in mind, DNS results are becoming more and more important as numerical test cases for transition because they eliminate a lot of the uncertainty that is present in the experimental transition results. For example, the effect of the freestream turbulent length scale on the transition onset location is completely ignored in the present empirical correlations (primarily because it is rarely measured in the experiments) and this effect is thought to be the largest source of error in the present results. A DNS study that quantifies the effect of freestream length scale on the transition location would go a long way towards reducing some of the uncertainty in the present empirical correlations.

To conclude, the current formulation would appear to be a significant step forward in engineering transition modelling, as it allows the combination of transition correlations with general purpose CFD codes. The present model formulation is very likely a starting point for the inclusion of numerous additional effects and flow regimes such as roughness, freestream turbulent length scale, streamline curvature, cross-flow transition and Mach number effects. There is a strong potential that the model will allow the 1st order effects of transition to be included in everyday industrial CFD simulations.

References

Abu-Ghannam, B.J. and Shaw, R., 1980, "Natural Transition of Boundary Layers -The Effects of Turbulence, Pressure Gradient, and Flow History," *Journal of Mechanical Engineering Science*, Vol. 22, No. 5, pp. 213 – 228.

Achenbach, E., 1968, "Distribution of Local Pressure and Skin Friction around a Circular Cylinder in Cross-flow up to Re=5 x 10^6" *Journal of Fluid Mechanics*, Vol. 34, pp. 648–654.

Arts, T., Lambert de Rouvroit, M., Rutherford, A.W., 1990, "Aero-Thermal Investigation of a Highly Loaded Transonic Linear Turbine Guide Vane Cascade", von Karman Institute for Fluid Dynamics, Technical Note 174.

Barth, T.J. and Jesperson, D.C., 1989, "The design and application of upwind schemes on unstructured meshes", AIAA Paper 89-0366.

Biswas, D. and Fukuyama, Y., 1994, "Calculation of Transitional Boundary Layers With an Improved Low-Reynolds-Number Version of the k-ε Turbulence Model," ASME *Journal of Turbomachinery*, Vol. 116, pp. 765 - 773.

Chaput, E., 1997, "Chapter 3: Application-Oriented Synthesis of Work Presented in Chapter II", *Notes on Numerical Fluid Mechanics*, Vol. 58, Vieweg Braunschweig. Wiesbaden, pp. 327-346.

Cho, N.H., Liu, X, Rodi, W., Schönung, B., 1993, "Calculation of Wake-Induced Unsteady Flow in a Turbine Cascade", ASME *Journal of Turbomachinery*, Vol. 115, pp. 675 - 686.

Crouch, J.D., 1997, "Transition Prediction and Control for Airplane Applications", AIAA Paper 97-1907.

Crouch, J.D. and Ng, L.L., 2000, "Variable N-Factor Method for Transition Prediction in Three-Dimensional Boundary Layers", *AIAA Journal*, Vol. 28, No. 2, Feb., pp 211-216.

Dhawan, D. and Narasimha, R., 1958, "Some Properties of Boundary Layer Flow During Transition from Laminar to Turbulent Motion", *Journal of Fluid Mechanics*, Vol. 3, pp. 418-436.

Dong, Y. and Cumpsty, N.A., 1990, "Compressor Blade Boundary Layers: Part I, the Test Facility and Measurements with no Incident Wakes", ASME *Journal of Turbomachinery*, Vol. 112, pp. 222 – 231.

Dong, Y. and Cumpsty, N.A., 1990, "Compressor Blade Boundary Layers: Part 2—Measurements With Incident Wakes", ASME *Journal of Turbomachinery,* Vol. 112, pp. 231–240.

Dorney, D.J., Lake, J.P., King, P.L. and Ashpis, D.E., 2000, "Experimental and Numerical Investigation of Losses in Low-Pressure Turbine Blade Rows," AIAA Paper AIAA-2000-0737, Reno, NV.

Drela, M., and Giles, M. B., 1987, "Viscous-Inviscid Analysis of Transonic and Low Reynolds Number Airfoils", *AIAA Journal*, Vol. 25, pp. 1347 – 1355.

Drela, M., 1995, "MISES Implementaion of Modified Abu-Ghannam/Shaw Transition Criterion", MIT Aero-Astro.

Durbin, P.A., Jacobs, R.G. and Wu, X., 2002, "DNS of Bypass Transition," *Closure Strategies for Turbulent and Transitional Flows*, edited by B.E. Launder and N.D. Sandham, Cambridge University Press, pp. 449-463.

Emmons, H.W., 1951, "The Laminar-Turbulent Transition in a Boundary Layer – Part 1", Journal of Aerospace Science, Vol. 18, No 7, pp 490-498.

Eulitz, F. and Engel, K., 1998, "Numerical Investigation of Wake Interaction in a Low-Pressure Turbine", ASME Paper GT98-563.

Fashifar, A. and Johnson, M. W., 1992, "An Improved Boundary Layer Transition Correlation", ASME Paper ASME-92-GT-245.

Germano, M., Piomelli, U., Moin, P., Cabot, W.H., 1991, "A Dynamic Subgrid-Scale Eddy Viscosity Model", Physics of Fluids A 3, Number 7, pp. 1760-1765.

Gostelow, J.P., Blunden, A. R., and Walker, G. J., 1994, "Effects of Freestream Turbulence and Adverse Pressure Gradients on Boundary Layer Transition," *ASME Journal of Turbomachinery*, Vol. 116, pp. 392-404.

Grotjans, H. and Menter, F.R, 1998, "Wall Functions for General Application CFD Codes", Computational Fluid Dynamics, Proceedings of the 4th Computational Fluid Dynamics conference, 7-11 Sept. 1998, Athens, Greece, Vol. 1, Part 2, ECCOMAS, pp. 1112-1120.

Haase, W., Chaput, E., Elsholz, E., Leschziner, M. and Mueller, U.R., 1997, "ECARP – European Computational Aerodynamics Research Project: Validation of CFD Codes and Assessment of Turbulence Models", Notes on Numerical Fluid Mechanics, Vol. 58

Halstead, D. E., Wisler, D. C., Okiishi, T. H., Walker, G. J., Hodson, H. P., and Shin, H.W., 1997, "Boundary Layer Development in Axial Compressors and Turbines: Parts 1–

4”, ASME *Journal of Turbomachinery*, Vol. 119, pp. 114–127, pp. 426–444, pp. 234–246 and pp. 128–139.

Huang, J., Corke, T.C., Thomas, F.O., 2003, “Plasma Actuators for Separation Control of Low Pressure Turbine Blades”, AIAA Paper No. AIAA-2003-1027.

Howell, R.J., Ramesh, O.N., Hodson, H.P., Harvey, N.W. and Schulte, V., 2001, “High Lift and Aft-Loaded Profiles for Low-Pressure Turbines”, ASME *Journal of Turbomachinery*, Vol. 123, pp. 181-188.

Jones, W. P., and Launder, B. E., 1973, “The Calculation of Low Reynolds Number Phenomena with a Two-Equation Model of Turbulence”, *Int. J. Heat Mass Transfer*, Vol. 15, pp. 301-314.

Klausmeyer, S.M. and Lin, J.C., 1997, “Comparative Results From a CFD Challenge Over a 2D Three-Element High-Lift Airfoil”, NASA Technical Memorandum 112858.

Klebanoff, P.S. and Tidstrom, K.D., Sargent, L.M., 1962, “The Three-Dimensional Nature of Boundary Layer Instability”, *Journal of Fluid Mechanics*, Vol. 12, pp. 1-24

Lardeau, S., Leschziner, M.A. and Li, N., 2004, “Modelling Bypass Transition with Low-Reynolds-Number Nonlinear Eddy-Viscosity Closure”, *Flow, Turbulence and Combustion,* Kluwer Academic Publishers.

Langtry, R.B., 2002, “Prediction of Transition for Attached and Separated Shear Layers in Turbomachinery”, Master of Applied Science Thesis, Carleton University.

Langtry, R.B., and Sjolander, S.A., 2002, “Prediction of Transition for Attached and Separated Shear Layers in Turbomachinery”, AIAA Paper 2002-3643.

Langtry, R.B., Menter, F.R., Likki, S.R., Suzen, Y.B., Huang, P.G., and Völker, S., 2004, "A Correlation based Transition Model using Local Variables Part 2 - Test Cases and Industrial Applications”, ASME Paper GT2004-53452.

Langtry, R.B. and Menter, F.R., 2005., “Transition Modeling for General CFD Applications in Aeronautics”, AIAA Paper 2005-522, Reno, Nevada.

Mary, I. and Sagaut, P., 2002, “Large Eddy Simulation of Flow Around an Airfoil Near Stall”, *AIAA Journal,* Vol. 40, No. 6, pp 1139-1145.

Mayle, R.E., 1991, “The Role of Laminar-Turbulent Transition in Gas Turbine Engines,” *Journal of Turbomachinery*, Vol. 113, pp. 509-537.

Mayle, R.E. and Schulz, A. 1997, “The Path to Predicting Bypass Transition,” ASME *Journal of Turbomachinery*, Vol. 119, pp. 405-411.

Malkiel, E. and Mayle, R.E., 1996, "Transition in a Separation Bubble," ASME *Journal of Turbomachinery*, Vol. 118, pp. 752-759.

Menter, F.R. and Esch, T., 2001, "Elements of Industrial Heat Transfer Predictions; presented at the 16th Brazilian Congress of Mechanical Engineering (COBEM), Nov. 2001, Uberlandia, Brazil.

Menter, F.R., Esch, T. and Kubacki, S., 2002, "Transition Modelling Based on Local Variables", 5th International Symposium on Engineering Turbulence Modelling and Measurements, Mallorca, Spain.

Menter, F.R., 1994, "Two-Equation eddy-viscosity turbulence models for engineering applications", *AIAA Journal*, Vol. 32, No. 8, pp. 1598-1605

Menter, F.R., Langtry, R.B., Likki, S.R., Suzen, Y.B., Huang, P.G., and Völker, S., 2004, "A Correlation based Transition Model using Local Variables Part 1- Model Formulation", ASME-GT2004-53452, ASME TURBO EXPO 2004, Vienna, Austria.

Michelassi, V., Wissink, J.G., Fröhlich, J., Rodi, W., 2003, "Large Eddy Simulation of Flow around a Turbine Blade with Incoming Wakes**",** *AIAA Journal*. Vol. 41, no. 11, pp. 2143-2156. Nov. 2003.

Morkovin, M.V., 1969, "On the Many Faces of Transition", *Viscous Drag Reduction*, C.S. Wells, ed., Plenum Press, New York, pp 1-31.

Pecnik, R., Sanz, W., Gehrer, A., Woisetschläger, J., 2003, "Transition Modeling Using two Different Intermittency Transport Equations", Flow Turbulence and Combustion, Vol. 70, pp. 299-323.

Nuernberger, D., and Greza, H., 2002, "Numerical Investigation of Unsteady Transitional Flows in Turbomachinery Components Based on a RANS Approach", *Flow Turbulence and Combustion*, Vol. 69, pp. 331-353.

Raw, M.J., 1996, "Robustness of coupled algebraic multigrid for the Navier-Stokes equations", AIAA Paper 96-0297.

Rhie, C.M. and Chow, W.L., 1983, "Numerical study of the turbulent flow past an airfoil with trailing edge separation", *AIAA Journal*, Vol. 21, pp. 1525-1532.

Rodi, W. and Scheuerer, G., 1984, "Calculation of Laminar-Turbulent Boundary Layer Transition on Turbine Blades", *AGARD CP 390 on Heat transfer and colloing in gas turbines*.

Rumsey, C.L., Gatski, T.B., Ying, S.X. and Bertelrud,A., 1998, "Prediction of High-Lift Flows Using Turbulent Closure Models" *AIAA Journal*, Vol. 36, No. 5.

Schmidt, R.C., Patankar, S.V. 1991, "Simulating Boundary Layer Transition with Low-Reynolds-Number k-e Turbulence Models: Part 1-An Evaluation of Prediction Characteristics," ASME *Journal of Turbomachinery,* vol. 113, pp. 10-17.

Schneider, G.E. and Raw. M.J., 1987, "Control volume finite-element method for heat transfer and fluid flow using collocated variables", 1. *Computational procedure. Numerical Heat Transfer*, pp 363-390.

Savill, A.M., 1993, Some recent progress in the turbulence modeling of by-pass transition, *In: R.M.C. So, C.G. Speziale and B.E. Launder, Eds.: Near-Wall Turbulent Flows*, Elsevier, p. 829.

Savill, A.M., 1996, One-point closures applied to transition, Turbulence and Transition Modeling, *M. Hallbäck et al., eds., Kluwer,* pp. 233-268.

Savill, A.M., 2002, "New Strategies in Modelling By-Pass Transition," *Closure Strategies for Turbulent and Transitional Flows*, edited by B.E. Launder and N.D. Sandsam, Cambridge University press, pp. 464-492.

Savill, A.M., 2002, "By-pass Transition using Conventional Closures," *Closure Strategies for Turbulent and Transitional Flows*, edited by B.E. Launder and N.D. Sandsam, Cambridge University press, pp. 464-492.

Schiele, R., 1999, "Die Transitionale Grenzschicht an Gasturbineneshaufeln: Experimentell Untersuchungen und Entwicklung eines neuen Verfahrens zur numerischen Beschreibung des laminar-turbulenten Umschlags", PhD Thesis, Universität Karlsruhe.

Schlichting, H., 1979, *Boundary Layer Theory*, McGraw-Hill, 7th edition.

Schubauer, G.B. and Skramstad, H.K., 1948, "Laminar-boundary-layer oscillations and transition on a flat plate," NACA Rept. 909.

Schubauer, G.B. and Klebanoff, P.S., (1955), "Contribution on the Mechanics of Boundary Layer Transition," NACA TN 3489.

Schulz, H.D., Gallus, H.D., 1988, "Experimental Investigation of the Three-Dimensional Flow in an Annular Compressor Cascade", ASME *Journal of Turbomachinery*, Vol. 110, October.

Schlichting, H., 1979, *Boundary Layer Theory*, McGraw-Hill, Inc.

Sinclair, C. and Wells, Jr., 1967, "Effects of Freestream Turbulence on Boundary-Layer Transition," *AIAA Journal*, Vol. 5, No. 1, pp. 172-174.

Sieger, K., Schiele, R., Kaufmann, F., Wittig, S. and Rodi, W., 1995, "A Two-Layer Turbulence Model for the Calculation of Transitional Boundary-Layers", ERCOFTAC bulletin 24, pp. 44-47.

Simms, D., Schreck, S., Hand, M, and Fingersh, L.J., 2001, "NREL Unsteady Aerodynamics Experiment in the NASA-Ames Wind Tunnel: A Comparison of Predictions to Measurements.", *NREL Technical report, NREL/TP-500-29494.*

Smagorinsky, J., 1963, Monthly Weather Revue, Vol. 91, No. 3, pp. 99–164.

Smith, A.M.O. and Gamberoni, N., 1956, "Transition, Pressure Gradient and Stability Theory," Douglas Aircraft Company, Long Beach, Calif. Rep. ES 26388.

Sobieczky, H., 1994, "DLR – F5: Test Wing for CFD and Applied Aerodynamics", Test Case B-5 in *AGARD FDP Advisory Report AR 303: Test Cases for CFD Validation*.

Steelant, J., and Dick, E., 2001, "Modeling of Laminar-Turbulent Transition for High Freestream Turbulence", *Journal of Fluids Engineering*, Vol. 123, pp. 22-30.

Stieger, R., Hollis, D., and Hodson, H., 2003, "Unsteady Surface Pressures due to Wake Induced Transition in a Laminar Separation Bubble on a LP Turbine Cascade" ASME-GT2003-38303, ASME TURBO EXPO 2003, Atlanta, Georgia.

Stock, H.W., 2006, "e^N Transition Prediction in Three-Dimensional Boundary Layers on Inclined Prolate Spheroids", AIAA Journal, Vol. 44, No. 1, pp. 108 – 118.

Stock, H.W. and Haase, W., 2000, "Navier-Stokes Airfoil Computations with e^N Transition Prediction Including Transitional Flow Regions," AIAA Journal, Vol. 38, No. 11, pp. 2059 – 2066.

Suzen, Y.B**.**, Huang, P.G., Hultgren, L.S., Ashpis, D.E., 2003, "Predictions of Separated and Transitional Boundary Layers Under Low-Pressure Turbine Airfoil Conditions Using an Intermittency Transport Equation," *Journal of Turbomachinery*, Vol. 125, No. 3, July 2003, pp. 455-464.

Suzen, Y.B., Huang, P.G., Volino, R.J., Corke, T.C., Thomas, F.O., Huang, J., Lake, J.P., King, P.I., 2003, "A Comprehensive CFD Study of Transitional Flows in Low-Pressure Turbines Under a Wide Range of Operating Conditions", AIAA-2003-3591, 33rd AIAA Fluid Dynamics Conference, Orlando, FL, June 2003.

Suzen, Y.B. and Huang, P.G., Private Communication, University of Kentucky, 2004.

Tain, L., and Cumpsty, N.A., 2000, "Compressor Blade Leading Edges in Subsonic Compressible Flow", *Journal of Mechanical Engineering Science*, Proc. Institution of Mechanical Engineers, Vol. 214 Part C, pp. 221–242.

Thermann, H., Müller, M., and Niehuis, R., 2001, "Numerical Simulation of the Boundary Layer Transition in Turbomachinery Flows,", ASME paper 2001-GT-0475.

Ubaldi, M., Zunino, P., Campora, U. and Ghiglione, A., 1996, "Detailed Velocity and Turbulence Measurements of the Profile Boundary Layer in a Large Scale Turbine Cascade", International Gas Turbine and Aeroengine Congress and Exhibition, Birmingham, UK, ASME 96-GT-42.

Van Ingen, J.L., 1956, "A suggested Semi-Empirical Method for the Calculation of the Boundary Layer Transition Region," Univ. of Delft, Dept. Aerospace Engineering, Delft, The Netherlands, Rep. VTH-74.

Van Driest, E.R. and Blumer, C.B., 1963, "Boundary Layer Transition: Freestream Turbulence and Pressure Gradient Effects," *AIAA Journa*l, Vol. 1, No. 6, June 1963, pp. 1303-1306.

Walters, D.K and Leylek, J.H., 2002, "A New Model for Boundary-Layer Transition Using a Single-Point Rans Approach", ASME IMECE'02, IMECE2002-HT-32740.

Walraevens, R.E. and Cumpsty, N.A., 1995, "Leading Edge Separation Bubbles on Turbomachine Blades", ASME *Journal of Turbomachinery*, Vol. 117, January 1995, pp. 115-125

Wang, M., Catalano, P. and Iccarino, G., 2001, "Prediction of High Reynolds Number Flow over a Circular Cylinder using LES with Wall Modeling,", Center for Turbulence Annual Research Briefs.

Warren, E.W. and Hassan, H.A. 1997, "Alternative to the e^n Method for Determining Onset of Transition," *AIAA Journal*, Vol. 36, No.1, pp. 111-113.

Wilcox, D.C., 1993*, Turbulence modeling for CFD*, DCW Industries, La Canada, Ca.

Wu, X., and Durbin, P.A., 2001, "Evidence of Longitudinal Vortices Evolved from Distorted Wakes in a Turbine Passage", Journal of Fluid Mechanics, Vol. 446, pp. 199-228

Youngren, H., and Drela, M., 1991, "Viscous-Inviscid Method for Preliminary Design of Transonic Cascades", AIAA Paper No. 91-2364.

Zheng, X., Liu, C., Liu, F., and Yang, C., 1998, "Turbulent Transition Simulation Using the k-w Model," *International Journal for Numerical Methods in Engineering*, Vol. 42, pp. 907-926.

Zierke, W.C. and Deutsch, S., 1989, "The measurement of boundary layers on a compressor blade in cascade – Vols. 1 and 2", NASA CR 185118.

Appendix:
Best Practice Guidelines for Using the Transition Model

This section is intended to provide new users of the transition model with some basic guidelines for using the transition model successfully. These best practice guidelines are based primarily on the experience gained largely over the development phase of the transition model.

1.0 Estimating when the Transition Model Should be Used

Because the transition model requires the solution of two extra transport equations there are additional CPU costs associated with using it. A rough estimate is that for the same grid the transition model solution requires approximately 18 percent additional CPU time compared to a fully turbulent solution. As well, the transition model requires somewhat finer grids than are typically used for routine design purposes. This is because the max grid y^+ must be approximately equal to one (i.e. wall-function grids cannot be used because they cannot properly resolve the laminar boundary layer) and sufficient grid points in the streamwise direction are needed to resolve the transitional region. For this reason it is important to be able to estimate when the additional cost of using the transition model in terms of CPU and grid generation time is justified. The relative percentage of laminar flow on a device can be estimated using the following formula, which is based on the Mayle (1991) empirical correlation for transition onset.

$$\frac{\mathrm{Re}_{xt}}{\mathrm{Re}_{x}} = \frac{380000 \cdot (100 \cdot Tu)^{-\frac{5}{4}}}{(\rho / \mu) \cdot V \cdot L_{Device}}$$

Where Re_{xt} is the transition Reynolds number, Re_x is the device Reynolds number, L_{Device} is the length of the device, V is a representative velocity, and Tu is the freestream turbulence intensity, which can be calculated as follows.

$$Tu = \frac{(2k/3)^{0.5}}{V}$$

where k is the turbulent kinetic energy. The fraction of laminar flow for some representative devices is shown in Table A.1. Clearly, there are many cases where the assumption of fully turbulent flow is not correct and a significant amount of laminar flow could be present.

It should be noted the above estimate does not account for the effect of pressure gradient, which can have a significant effect on the transition location, particularly if it results in a

laminar separation. In addition, the importance of the transition is not simply related to the length of the turbulent region. A tiny separation bubble close to the leading edge which reattaches can have a large effect on the performance as shown by Tain and Cumpsty (2000). This is because the size of a leading edge laminar separation bubble can have a dramatic effect on the downstream boundary layer thickness and hence the likely hood of the boundary layer separating, even if it has already transitioned to fully turbulent flow. This in turn can have a profound effect on the predicted losses or drag.

Case	Re_X	Tu (%)	Fraction Laminar Flow
LP Turbine blade	150 000	2.5	0.80
HP Turbine blade	500 000	6.0	0.10
Compressor blade	1 000 000	1.0	0.38
Small Aircraft	5 000 000	0.2	0.57
F1 Race Car Spoiler	2 000 000	0.3	0.86

Table A.1 Fraction of laminar flow for a variety of different devices.

2.0 Grid Requirements

The effect of increasing and decreasing y^+ for the T3A flat plate test case is shown in Figures A.1 and A.2. For y^+ values between 0.001 and 1 there is almost no effect on the solution. Once the maximum y^+ increases above 8 the transition onset location begins to move upstream. At a maximum y^+ of 25 the boundary layer is almost completely turbulent. For y^+ values below 0.001 the transition location appears to move downstream. This is presumably caused by the large surface value of omega, which scales with the first grid point height. Additional simulations on the Zierke compressor [23] have indicated that at very small y^+ values the SST blending functions switch to k-e in the boundary layer. For these reasons very small (below 0.001) y^+ values should be avoided. This is not a major concern because such small values would lead to grids that would be far too large to be practical for engineering purposes and below a value of 1 the is no significant improvement in the accuracy.

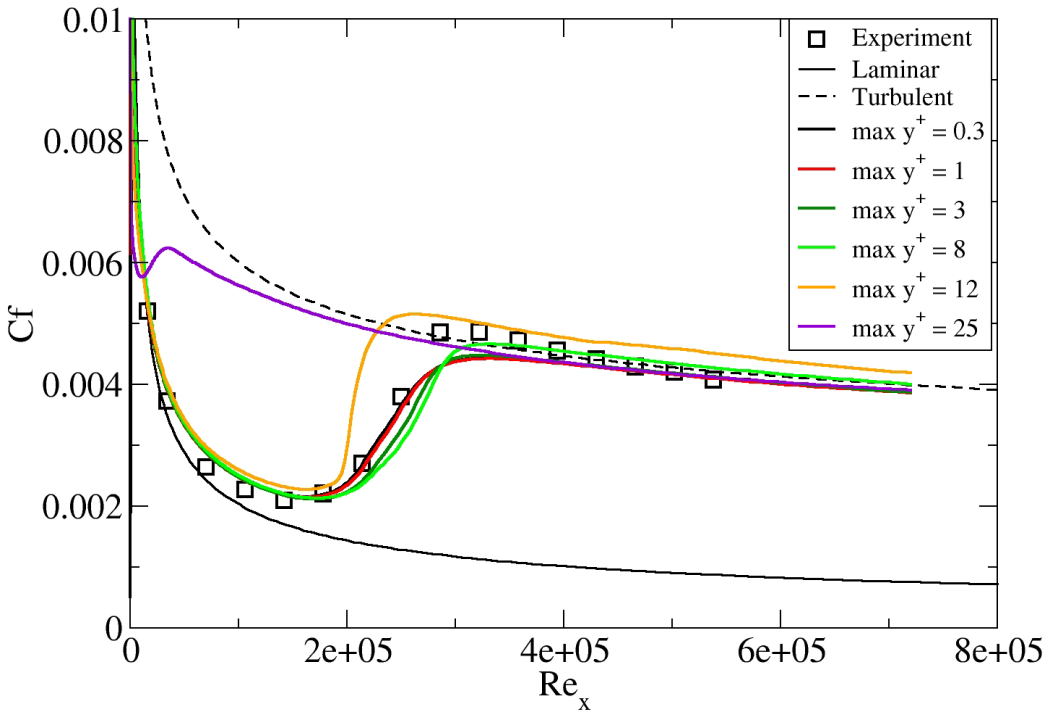

Figure A.1 Effect of increasing y^+ for the flat plate T3A test case.

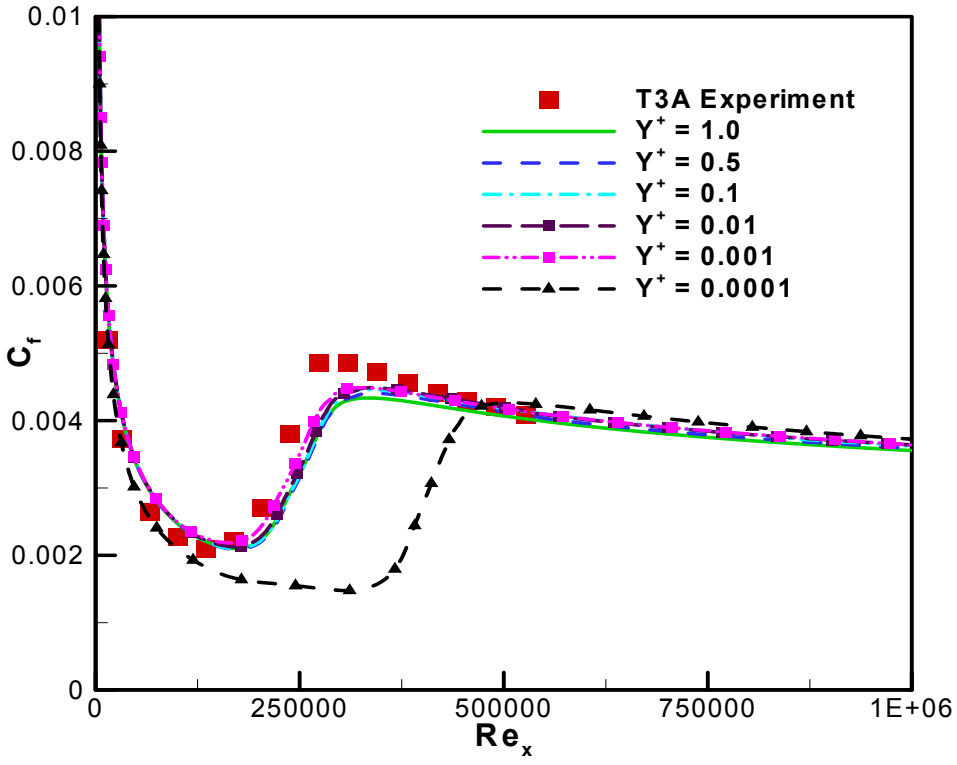

Figure A.2 Effect of decreasing y^+ for the flat plate T3A test case.

The effect of wall normal expansion ratio from a y^+ value of 1 is shown in Figure A.3. For expansion factors of 1.05 and 1.1 there is no effect on the solution. For larger expansion factors of 1.2 and 1.4 there is a small but noticeable upstream shift in the transition location.

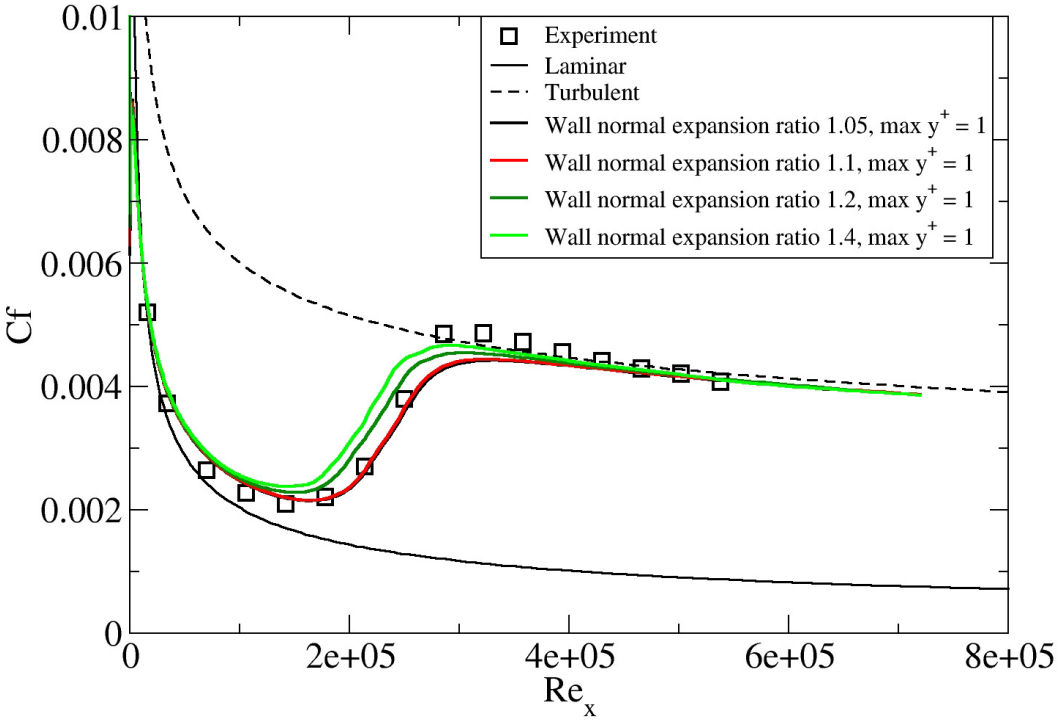

Figure A.3 Effect of wall normal expansion ratio for the flat plate T3A test case.

The effect of streamwise grid refinement is shown in Figure A.4. Surprisingly the model does not show a strong sensitivity to the number of streamwise nodes. The solution differed significantly from the grid independent one only for the case of 25 streamwise nodes where there was only one cell in the transitional region. Nevertheless the grid independent solution appears to occur when there is approximately 75 – 100 streamwise grid points from the leading edge to the trailing edge (i.e. one chord length). As well, separation induced transition occurs over a very short length and for cases where this is important a fine grid is necessary. Note that the high-resolution second order bounded discritization scheme has been used for all equations including the turbulent and transition equations and this is the recommended default setting for transitional computations. In CFX when the transition model is active and the high-resolution scheme is selected for the hydrodynamic equations the default advection scheme for the turbulence and transition equations is automatically set to high resolution.

One point to note is that for sharp leading edges often transition can occur at the leading edge due to a small leading edge separation bubble. If the grid is too course, the rapid transition caused by the separation bubble is not captured. A good example of this is the

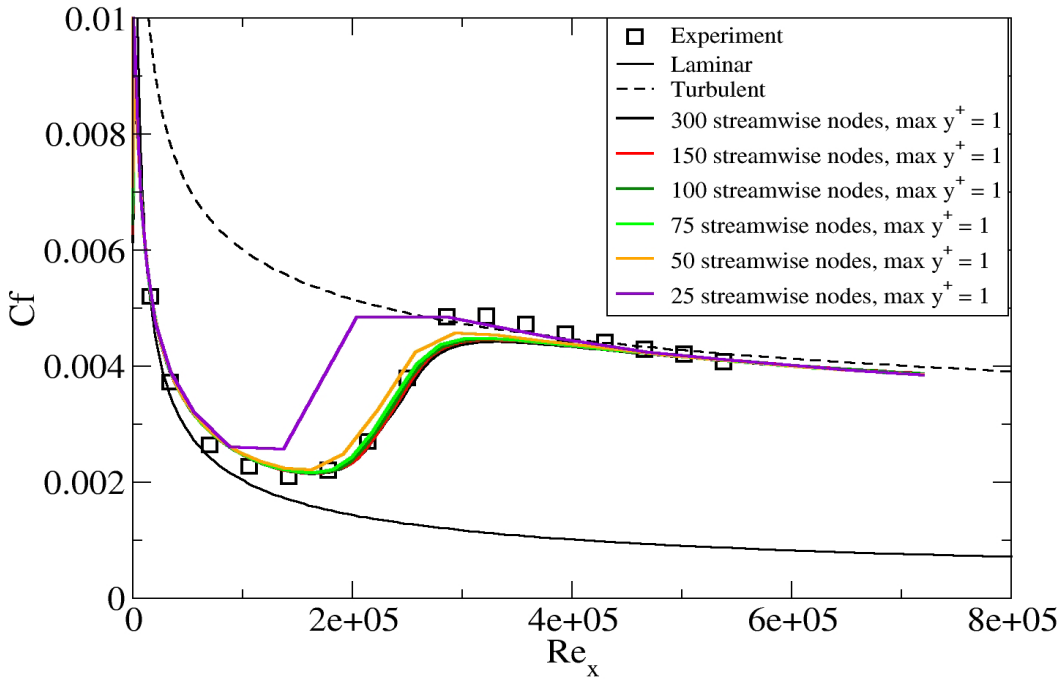

Figure A.4 Effect of streamwise grid density for the flat plate T3A test case.

Zierke compressor. Contours of velocity (top) and turbulence intensity (Tu, bottom) for the Zierke compressor are shown in Figure A.5. On the suction side transition occurs at the leading edge due to a small leading edge separation bubble. On the pressure side transition occurs at about mid-chord. The effect of stream-wise grid resolution on resolving the leading edge laminar separation and subsequent transition on the suction side is shown in Figure A.6. Clearly, if there are not a large enough number of streamwise nodes, the model cannot resolve the rapid transition and a laminar boundary layer on the suction side is the result.

Based on the grid sensitivity study the recommended best practice mesh guidelines are a max y^+ of 1, a wall normal expansion ratio of 1.1 and about 75 – 100 grid nodes in the streamwise direction. Note that if separation induced transition is present additional grid points in the streamwise direction are most likely needed. For a typical 2-D blade assuming an H-O-H type grid the above guide lines result in an inlet H-grid of 15x30, an O-grid around the blade of 200x80 and an outlet H-grid of 100x140 for a total of approximately 30 000 nodes (note that CFX-5 is not a 2D code, thus this estimate jumps to 60 000 for a one cell, 2 node thick grid), which has been found to be grid independent for most turbomachinery cases. It should also be noted that for the surfaces in the out of plane z-direction symmetry planes should always be used, not slip walls. The use of slip walls has been found to result in an incorrect calculation of the wall distance, which is critical for calculating the transition onset location accurately. Another point to note is that all the validation cases for the transition model have been performed on hexahedral meshes. At this point the accuracy of the transition model on tetrahedral meshes has not been investigated.

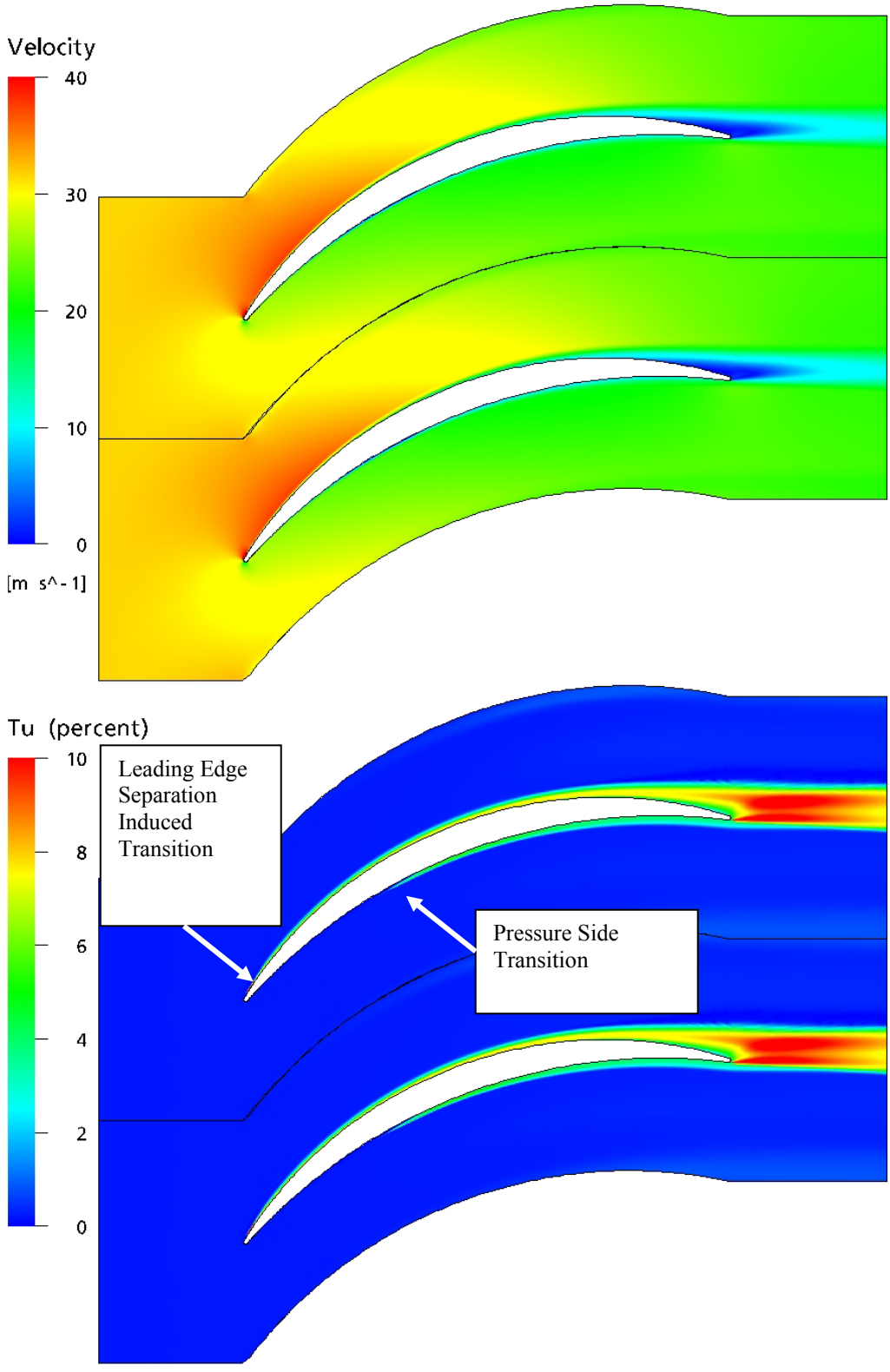

Figure A.5 Contours of velocity (top) and turbulence intensity (Tu, bottom) for the Zierke compressor.

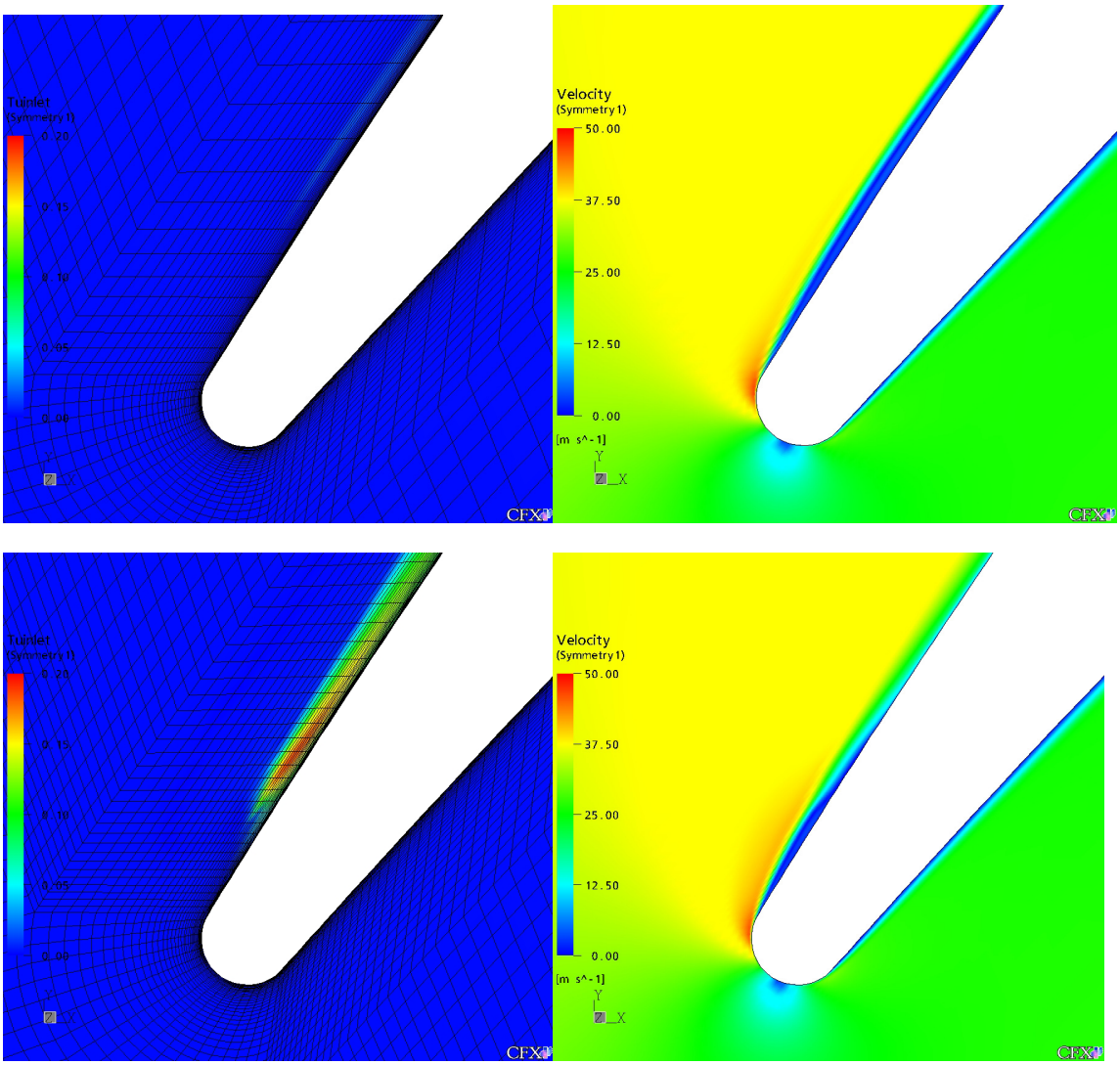

Turbulence Intensity **Velocity**

Figure A.6 Effect of stream-wise grid resolution (coarse grid, top), (fine grid, bottom), for resolving transition due to a leading edge separation bubble for the Zierke compressor.

3.0 Specifying Inlet Turbulence Levels

It has been observed that the turbulence intensity specified at an inlet can decay quit rapidly depending on the inlet viscosity ratio (μ_t/μ) (and hence turbulence eddy frequency). As a result, the local turbulence intensity downstream of the inlet can be much smaller than the inlet value (see Figure A.7). Typically, the larger the inlet viscosity ratio the smaller the turbulent decay rate. However, if too large a viscosity ratio is specified (i.e. >100) the skin friction can deviate significantly from the laminar value. There is experimental evidence that suggests that this effect occurs physically, however at this point it is not clear how accurately the transition model reproduces this behavior. For this reason, if possible it is desirable to have a relatively low (i.e. ≈ 1 - 10) inlet viscosity ratio and to estimate the inlet value of turbulence intensity such that at the leading edge of the blade/airfoil the turbulence intensity has decayed to the desired value.

The decay of turbulent kinetic energy can be calculated with the following analytical solution.

$$k = k_{inlet} \cdot \left(1 + \omega_{inlet} \cdot \beta \cdot t\right)^{-\frac{\beta^*}{\beta}} \qquad \text{A.1}$$

For the SST turbulence model in the freestream the constants are:

β=0.09 β^*=0.0828

The time scale can be determined as follows:

$$t = \frac{x}{V}$$

where x is the streamwise distance downstream of the inlet and V is the mean convective velocity. The eddy viscosity is defined as:

$$\mu_t = \frac{\rho k}{\omega}$$

The decay of turbulent kinetic energy equation can be rewritten in terms of inlet turbulence intensity (Tu_{inlet}) and eddy viscosity ratio (μ_t/μ) be substituting those relations into Equation A.1 as follows:

$$Tu = \left(Tu_{inlet}^{\,2} \left[1 + \frac{3 \cdot \rho \cdot V \cdot x \cdot \beta \cdot Tu_{inlet}^{\,2}}{2 \cdot \mu\left(\mu_t / \mu\right)} \right]^{-\frac{\beta^*}{\beta}} \right)^{0.5} \qquad \text{A.2}$$

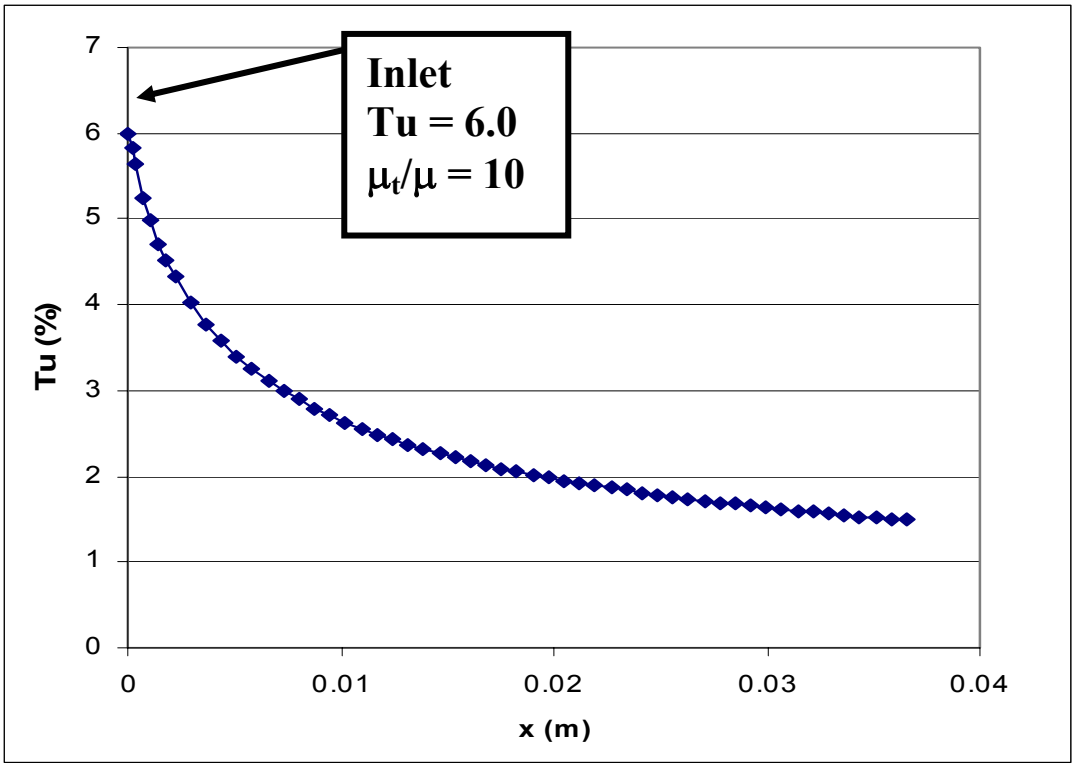

Figure A.7 Decay of turbulence intensity (Tu) as a function of streamwise distance (x).

4.0 Summary

This appendix has summarized the key issues required to successfully apply the new transition model. Proper grid refinement and specification of inlet turbulence levels is crucial for accurate transition prediction. In general there is some additional effort required during the grid generation phase because a low-Re grid with sufficient streamwise resolution is needed to accurately resolve the transition region. As well, in regions where laminar separation occurs, additional grid refinement is necessary in order to properly capture the rapid transition due to the separation bubble. Finally, the decay of turbulence from the inlet to the leading edge of the device should always be estimated before running a solution as this can have a large effect on the predicted transition location.

L E B E N S L A U F

Robin Langtry

Personalien:	Geburtstag:	29.01.1978
	Geburtsort:	Ottawa, Kanada
	Eltern:	Ross Langtry
		Heather Roy
	Eheschliessung:	29.12.2004
		Stacie Langtry geb. Burchell
Schulausbildung	1984 – 1988	Severn Avenue Public School
	1988 – 1992	D. Roy Kennedy Public School
	1992 – 1993	Nepean High School
	1993 – 1996	Woodruff High School
Studium:	1996 – 2000	B. Eng. Aerospace, Carleton University
	2000 – 2002	M.A.Sc. Aerospace, Carleton University
Industrietätigkeit:	1999	Internship, Canadian Space Agency
	2002 – 2006	Project Engineer, ANSYS CFX Germany GmbH